Surface Studies of Cobalt-Manganese Oxide and Industrial Iron Catalysts used in the Fischer-Tropsch Synthesis.

Mark Justin Betts

Submitted for the degree of Master of Science
University of the Witwatersrand, Johannesburg
September 1989

Abstract

The surfaces of pure and potassium promoted cobalt-manganese oxide as well as iron-based catalysts have been characterised before and after various treatments.

The effects of reduction and carburisation of cobalt-manganese oxide catalyst surfaces is reported. CO-hydrogenation over pure and potassium-promoted cobalt-manganese oxide was also undertaken. Finally, various aspects of hydrogen sulphide poisoning of an industrial iron-based catalyst during CO-hydrogenation were investigated.

A miniature high pressure reactor (15 bar) interfaced to the UHV chamber and a gas chromatogram enabled "*in situ*" surface analysis by XPS and AES to be carried out between successive catalyst treatments, as well as monitoring of CO-hydrogenation product distributions.

The surface composition of the cobalt-manganese oxide catalysts was shown to differ considerably with respect to the bulk. There was significant depletion of surface cobalt, especially after reduction, and there was evidence to indicate that reduction of the cobalt was bulk initiated. Potassium segregated to the surface and inhibited efficient reduction of the surface cobalt in the Co/MnO catalyst. Pure CO re-oxidised the surface cobalt, reduced all the manganese to MnO, gave rise to graphite deposition, $CO_{2\ (ads)}$ at the surface and bulk carbide formation. Large quantities of light hydrogenated carbon or "C_xH_y" species were observed at the surface after CO-hydrogenation treatments, and a small amount of bulk-carbon was only detected with the potassium promoted Co/MnO. Both these factors serve as testimony to the higher hydrogenation activity and can also contribute to explaining the longer catalyst lifetimes shown by Co/MnO compared to Fe/MnO and industrial iron-based CO-hydrogenation catalysts. Small amounts of oxygenated carbon were also observed, and this was more pronounced over the potassium promoted catalyst.

H_2S selectively attacked the potassium when sulphur poisoning treatments were administered to an industrial iron-based catalyst between CO-hydrogenation treatments. Correlations between hydrocarbon selectivities, sulphur dosages and treatment conditions, as well as surface studies, enabled a theory on the possible mechanism of H_2S interaction with the catalyst to be proposed.

I declare that this dissertation is my own, unaided work. It is being submitted for the degree of Master of Science in the University of the Witwatersrand, Johannesburg. It has not been submitted before for any degree or examination in any other university.

1st day of September, 1989 .

In memory of my late father, Alf Betts.

Acknowledgements

I am extremely grateful to the following people and institutions:

Professor R.G. Copperthwaite, my supervisor for giving me the opportunity to undertake this work. Also for his guidance and assistance, as well as expert advice and help with interpretation of data collected throughout the course of this work.

My fellow student, Peter Loggenberg for taking the time to show and inform me as to the intricate operation of the experimental equipment. Also for his useful input and ideas, as well as making various diagrams of the equipment and a computer programme for curve fitting of XPS data available to me.

The staff of the Schonland Research Centre for Nuclear Sciences, especially the following.
Professor J.P.F. Sellschop and Dr. T.E. Derry for their input at work discussion meetings.
Professor H. Arnegarn and Lynn Heyns for their administration of matters financial.
Mick Rebak for the provision and attachment of a diamond to the sample holder in order to facilitate catalyst temperature measurements.
Hugo Andeweg, Gidu Goldstein and John Beer for their upkeep of various electronic components.

The Catalysis Research Programme at Wits, especially:
Mark van der Riet and Saul Colley, for providing me with catalyst samples.
Themi Themistocleous for performing TGA analyses.
David Innes, for helping with some of the final arrangements.

Sastech (Pty) Ltd and the Foundation for Research and Development for funding through the grants of Professor Copperthwaite, as well as the University for financial assistance.

Finally, I am most grateful to my family for all their support, especially my wife Adrienne, for her patience, inspiration and cooking.

CONTENTS

CHAPTER 4. CO-hydrogenation over cobalt-manganese oxide

CHAPTER 5. CO-hydrogenation over potassium promoted cobalt-manganese oxide

CHAPTER 4. CO-hydrogenation over cobalt-manganese oxide

CHAPTER 5. CO-hydrogenation over potassium promoted cobalt-manganese oxide

CHAPTER 6. H_2S poisoning over a fused iron-based CO-hydrogenation catalyst

List of Abbreviations

AES	Auger Electron Spectroscopy
AR	Analytical Reagent
BE	Binding Energy
BET	Brunauer-Emmet-Teller
CAE	Constant Analyser Energy
CLAM	Combined Lens Analyser Module
EDAX	Energy Dispersive Analysis of X-rays
ESCA	Electron Spectroscopy for Chemical Analysis
FID	Flame Ionisation Detector
F-T	Fischer-Tropsch
GC	Gas Chromatography
HPR	High Pressure Reactor
HPT	High Precision Translator
KE	Kinetic Energy
PIC	Photo-Ionisation Cross-section
r.s.a.p.	relative surface atomic percentage
TGA	Thermogravimetric Analysis
TCD	Thermal Conductivity Detector
UHP	Ultra High Purity
UHV	Ultra High Vacuum
XPS	X-ray Photoelectron Spectroscopy
XRF	X-ray Fluorescence

List of Figures

List of Tables

1. General Introduction

1.1. The CO-hydrogenation reaction (Fischer-Tropsch process)

In 1902 the first carbon monoxide - hydrogenation reaction was reported. Sabatier and Senderens passed carbon monoxide (CO) and and hydrogen (H_2) gas over cobalt and nickel and produced methane [1]. BASF later used high pressures of CO and H_2 along with cobalt catalysts to produce liquid products in 1913 [2].

It was not until the early 1920's when further work into CO-hydrogenation was undertaken by two Germans, Franz Fischer and Hans Tropsch, and interest in the subject was rekindled resulting in the Fischer-Tropsch (F-T) process. This well known and well reported process involves the reaction of steam and coal to produce synthesis gas (CO and H_2) and the subsequent catalysed reaction of this gas to form hydrocarbons. The technology was discovered in Germany and is named after the two scientists responsible for pioneering work in this field. Fischer and Tropsch's initial work reported the production of hydrocarbons and oxygenated derivatives using alkali treated iron shavings at high pressures [3]. Because these catalysts exhibited rapid deactivation, and a high tendency towards oxygenate production, further research in order to find a more viable catalyst was pursued. Zinc oxide was added to Fischer and Tropsch's original catalyst [4], and the use of lower reaction pressures was found to lower the oxygenated hydrocarbon selectivity, but short catalyst lifetimes were still a problem. This led to the use of the more expensive cobalt type catalysts which consisted mainly of Co,ThO_2 MgO and Kieselghur [5], (with relative mass units in the order of 100:5:8:200 respectively). Industrialisation of the process followed in 1936 and found large scale application in Germany during World War II. The discovery by Pichler in 1936 that the lifetime of iron catalysts is largely improved by the use of higher pressures [6] was not followed up by German firms during World War II. It was not until after the war that iron catalysts were used in commercial synthetic fuel plants.

Today the only commercial synthetic fuel plants in operation which are based on the F-T reaction are those owned by the SASOL company in South Africa, as the low oil price in the 1950's led to the closure of most of the then commercially operated plants in Europe and the United States. As was the case in Germany prior to World War II,

South Africa is inclined to pursue the synthetic fuels path for strategic and political reasons.

This is a very brief account of the development of the F-T process, there are however numerous books and reviews available on the topic which contain a substantial amount of information [6-9]. Other facets of the F-T process, including the industrial operation of F-T plants, as well as reactor types and operations, have been reviewed by Dry [5].

1.2. CO-hydrogenation mechanisms

Product distributions in F.T. synthesis are conveniently explained using the Schulz-Flory polymerisation model. The Schulz-Flory distribution is a combination of Schulz's equation for radical polymerisation of vinyl monomers [10], and Flory's linear condensation polymerisation expression [11]. The resulting equation is widely used in F-T catalysis for predicting hydrocarbon product distribution models. There are however cases where these models do not work, and looking at possible reaction mechanisms is then of value.

The F-T reaction mechanism, (or mechanisms) has been a topic of considerable debate with a number of different proposals being put forward. The most well known being the carbide, the hydroxy-carbene and the CO insertion mechanisms. Other mechanisms, including variations and combinations of the above have also been proposed.

The carbide mechanism involves CO dissociation prior to interaction with H_2 followed by insertion of a CH_x group from a M-CH_x unit so formed into the M-C bond, as was first proposed by Fischer and Tropsch [4]. They proposed a mechanism proceeding via hydrogenation of a metal carbide followed by polymerisation of these metal methylene complexes to form hydrocarbons. Product formation is via beta-elimination or hydrogenation resulting in cleavage of the M-C bond. This mechanism may be schematically represented as follows:

$$\begin{array}{c} C \\ | \\ M \end{array} \longrightarrow \begin{array}{c} CH_x \\ | \\ M \end{array} \longrightarrow \begin{array}{c} CH_2-R \\ | \\ M \end{array} \longrightarrow \text{hydrocarbons}$$

This mechanism has been extensively reviewed by Muetterties and Stein [12], Brady and Petit [13] [14], Hermann [15], Henrici-Olivé and Olivé [16], Roder and Werner [17] and others. Although there is considerable proof for the validity of the carbide mechanism, it does not fully explain all the products observed during F-T synthesis, especially oxygenated hydrocarbons.

The hydroxy-carbene mechanism involves CO adsorption onto the metal to form an M=C=O species which interacts with two M-H units to form the M-CHOH (or hydroxycarbene) intermediate. C-C bond formation then takes place via a condensation reaction involving two M-CHOH and two M-H units to produce $M{=}CCH_3OH$ and H_2O. This process continues and results in formation of an M=C(R)OH species. F-T product formation is facilitated by dehydration, along with hydrogenation, resulting in the formation of a hydrocarbon. Alternatively, desorption of the products is facilitated by hydrogenation of the intermediate to form an alcohol. The hydroxy-carbene mechanism may be schematically represented as follows:

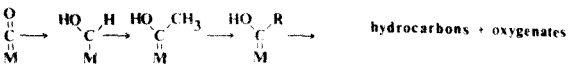

This mechanism was first developed and proposed by Storch, Golumbic and Anderson [7]. Kummer and Emmet [18], provided evidence that was shown to more successfully explain the observed F-T products. Variations of this mechanism where carbene or $M{=}CH_2$ intermediates also play a role have been proposed by Voevodski *et al.* [19], Hamai [20], and Ekstroom *et al.* [21].

The CO insertion mechanism involves CO insertion into the M-H bond of a $MH(CO)_x$ unit derived from the interaction of $M(CO)_x$ and H_2. The CO insertion is coupled to hydrogenation and results in a $MCH_3(CO)_{x-1}$ unit. $MCH_3(CO)_x$ is formed when another carbonyl is attached to the metal site. Hydrocarbon chain propagation then proceeds via further CO insertion into the M-C bond, resulting in $MCOR(CO)_{x-1}$ which can undergo a number of desorption reactions to form various oxygenates and hydrocarbons. The mechanism may schematically be represented as follows:

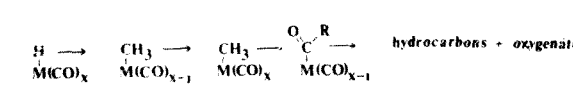

This mechanism was first put forward by Pichler and Schulz [22] and was derived from analogous homogeneous co-ordination chemistry. A common variation of this mechanism is the formyl mechanism whereby CO groups do not necessarily have to be on the same metal atom. This mechanism has been extensively reviewed by Muetterties and Stein [12], Rofer-De Poorter [23] and Henrici-Olivé and Olivé [16][24].

The three mechanisms thus far mentioned all discuss the type of C_1 species present, and not one can be discounted completely. To date the carbide mechanism has received the most support; however, the fact that the wide range of products observed during F-T synthesis differs with changing reaction conditions and different catalyst types, indicates that the process is far more complex. Thermodynamic and kinetic considerations must be taken into account and indeed more than one mechanism may be operating. Numerous other mechanisms have been proposed some of which combine more than one of the above general schemes and of special significance here are those reviewed by Dry [5].

1.3 Catalyst supports and promoters

Promoters and supports are added to catalysts in order to modify their activities by increasing the active surface area and/or changing the electronic properties of the catalyst so as to obtain a desired product distribution.

For an iron catalyst supported on alumina, the alumina has been termed a structural promoter [25], meaning that the role of the alumina is to enlarge the active iron surface area by inhibition of iron crystal growth [26]. An analagous effect can be expected with other non-reducable metal oxides, and according to Dry *et al.* [27], the effectiveness sequence of metal oxides in increasing the BET area is:

$$Al_2O_3 > TiO_2 > Cr_2O_3 > MgO > MnO = CaO > SiO_2 \simeq BeO$$

It is also well known that the stronger bases of the Group I metals, such as K_2O, are key promoter components in iron based catalysts in that they markedly effect both the catalyst activity and (especially) the selectivity. Such promoters that have a high "basicity" result in the catalyst surface having a higher electron density, which in turn modifies the catalyst's surface chemistry, and this has important consequences on the product distributions.

Promoters that are employed to modify the catalyst selectivity are termed "chemical" promoters. In most cases however, chemical promoters have a dual functionality in that they also contribute to increasing the active surface area, because most promoters employed in F-T synthesis catalysts are less readily reduced than the active metal centres. Basic alkalis readily form compounds with many of the commonly used supports such as silica and alumina [5].

In contrast to iron, the F-T synthesis performance of cobalt and ruthenium catalysts has been shown to be independent of the presence of chemical promoters when operating at high pressures [8], but when operating at atmospheric pressures, promotion with alkali and thoria increases wax production [5]. The main reason for incorporating supports with the early industrial cobalt and ruthenium F-T catalysts was therefore to increase catalyst activities by ensuring higher active surface areas [5].

1.4. Catalyst deactivation

Fischer-Tropsch catalysts may lose their activity as a result of a number of factors. These include; conversion of the active phase (metal) to an inert phase (oxide); loss of surface area due to crystallite growth (or sintering); loss of active surface area due to excessive build-up of carbonaceous material (or "fouling"); and finally, chemical poisoning of the surface (for example, by sulphur) [5].

The mechanism of deactivation by oxidation and sintering is well established, and both processes are facilitated by the presence of water vapour in F-T reactors. Oxidation and sintering of the catalyst are shown to occur due to prolonged use under normal F-T process conditions.

The effect of excessive carbon build-up or "fouling" also becomes critical with prolonged use of the catalyst in the F-T reactors. This fouling occurs due to wax build-up over the catalyst which in turn slows down the rate of diffusion of reactants, thereby slowing down the rate of reaction and hydrocarbon product formation.

Catalyst poisoning usually results from the presence of sulphur and sulphur containing compounds (for example, H_2S, COS and C_2H_5SH) in the F-T reactors. Due to the high sulphur content in South African coal, sulphur breakthroughs pose a problem at Sasol [28]. Sulphur has to be removed from the synthesis gas in a Rectisol or

scrubbing plant prior to being sent to the F-T reactors. Although it has long been known that sulphur compounds rapidly deactivate iron, nickel and cobalt catalysts the effect that alkali has on the mechanism by which this takes place is poorly understood. Since electronegative sulphur and sulphur compounds readily react with iron (to form FeS), and strong alkalis (for example, potassium and potassium compounds), one would expect that all electronegative species would act as poisons. This however is not the case, since fluoride ions do not have an adverse effect on the activity of iron catalysts, whereas bromide and chloride ions deactivate iron [5].

1.5. Surface characterisation and catalysis

In heterogeneous catalysis knowledge of the catalyst *surface* composition is essential in providing an informed picture of how the catalyst operates. This is especially true for F-T catalysis, as the surface is the region where feed gas is converted into useful hydrocarbon product. Furthermore, surface compositions often vary considerably with respect to bulk compositions. Surface segregation of different elements or molecules from the bulk phase occurs in most heterogeneous solids, particularly when they are subjected to elevated temperatures and pressures (as is the case in F-T catalysis). The surface is also the region where reaction intermediates can be observed, and this allows scope for mechanistic interpretations. It is also the region that must undergo changes during reduction since this activates the catalyst, and as well as during CO-hydrogenation, since the F-T product spectrum is known to change with reaction time over a given catalyst. The catalyst eventually loses activity, indicating that the catalyst surface composition must undergo changes as the F-T reaction proceeds.

It was not until the begining of the 1970's that scientists developed efficient ways for analysing surfaces at atomic levels. Numerous techniques exist today for the analysis of surfaces and there are a number of textbooks which review these [29-31]. Two of these techniques are relevant to the work in this dissertation, namely, X-ray photoelectron spectroscopy (XPS) and Auger electron spectroscopy (AES).

X-ray Photoelectron Spectroscopy

The XPS technique, also sometimes referred to as "ESCA" (or Electron Spectroscopy for Chemical Analysis) was pioneered by Siegbahn and his co-workers [32]

culminating in his winning a Nobel prize for physics in 1981. The principle underlying the XPS technique is simple. Briefly, monochromatic X-rays irradiate a solid surface causing photoelectrons to be liberated from their bound states. (See Figure 1.1). The kinetic energy (KE) of an emitted electron is directly proportional to it's core level binding energy (BE) when exposed to radiation of energy $h\nu$ by the relationship

$$BE = h\nu - KE - \phi \tag{1}$$

where ϕ is the photoelectron spectrometer work function.

Although X-rays are known to penetrate solids to appreciable depths it is the depth from which the photoelectrons are emitted without loss of energy that allows XPS to be used as a surface sensitive technique. The photoelectron escape depth is in the range of 10 to 20 A° [33] and is dependent on the electron kinetic energy [34]. The XPS signal can be shown to be comprised of approximately 30% from the outermost atomic layer with 60% coming from about the next three layers [33], when using normal X-ray sources. The XPS technique exploits chemical shift data to characterise surfaces. The "chemical shift" is the difference in binding energy of core level electrons due to atoms of the same element being chemically non-equivalent. Non-equivalence of atoms can arise in several ways namely, by differences in formal oxidation state, differences in molecular environment, differences in lattice site and so on. An important chemical shift consideration is the fact that the core level binding energy of electrons in a specific atom investigated increases as the electronegativity of the attached atom or groups increase. Along with chemical shift information, XPS also gives information as to the the ratios of atomic species at the surface. (See experimental chapter).

Shake-up satellites

Shake-up satellites are of particular relevence to the work in this dissertation, especially in the interpretation of various XPS spectra recorded. Basically, these structures are formed because valence electrons of atoms associate loss of a core electron with an increase in nuclear charge. This gives rise to a re-organisation of the valence electrons (referred to as relaxation) which may involve the electrons being excited to a higher valence level. (This process is known as a "shake-up"). The energy required for this transition is not available to the primary photoelectron and this leads to a discreet structure on the low KE side (or high BE) of the main photoelectron peak [31].

Auger Electron Spectroscopy

The AES technique is based on the detection of secondary electrons emitted from solid samples which are irradiated with an electron beam. These secondary (or Auger) electrons are named after the man who discovered them in 1925 [35]. An Auger electron is one which is emitted from an outer level of an atom with the same energy as that released by the filling of a core hole. The ability to scan small areas facilitated by the small electron beam width allows AES to be used as a microscopic surface tool. Although the technique does not impart as much chemical information as XPS, it is very useful for studying amorphous and inhomogeneous surfaces, especially when used in conjunction with XPS.

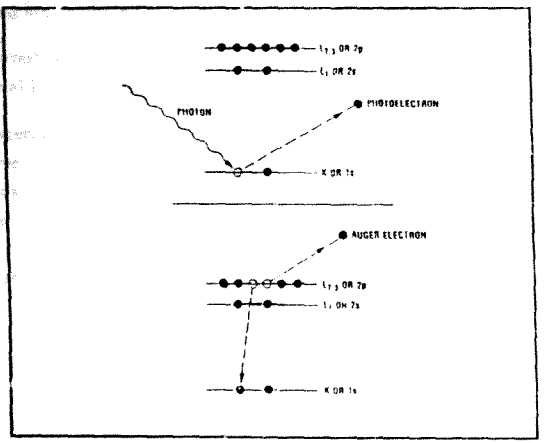

Figure 1.1. Diagram of the photoelectric process (top) and the Auger process (bottom).

1.6. Aims of this dissertation

The aim of the work undertaken was twofold:

1: To provide further insight into the functioning of cob .t-manganese oxide F-T catalysts.

Cobalt-manganese oxide catalysts have been developed and tested by the University of the Witwatersrand's catalysis research programme [36]. Cobalt-manganese oxide (Co/MnO) catalysts consisting originally of mixed oxides of cobalt and manganese are known to give rise to high short chain olefin yields when operating under certain F-T conditions [36]. The promotion of cobalt catalysts with MnO at low cobalt loadings, for example 5%, gives rise to high C_3 hydrocarbon selectivities [37]. Optimisation studies have shown that these catalysts can have high activity coupled to long lifetimes with respect to both industrial iron and iron-manganese oxide (Fe/MnO) catalysts, as well as giving high propene and low C_1 and C_2 hydrocarbon yields [36].

2: To investigate the interaction of sulphur (from hydrogen sulphide) with an iron-based industrial F-T catalyst.

More specifically, catalyst surfaces were studied by XPS and AES. The equipment used (see experimental section) enabled the surface to be characterised after successive reactions over the catalyst, or between successive treatments without the catalyst being exposed to ambient atmosphere. Products of reactions were determined by standard gas chromatography (or GC) techniques in order to facilitate correlations between hydrocarbon distributions and the surface composition of the catalysts.

Chapter 2. Experimental

2.1 Introduction

As mentioned in Chapter 1, photoelectron spectroscopy provides valuable information as to the chemical composition of the first few surface atomic layers of a solid. There are however problems associated with studying the surfaces of "working" heterogeneous catalysts. To give a good reflection of the catalyst's state under reaction conditions, the sample should be prepared under conditions as close as possible to "real" catalytic ones. This includes the period during which the sample is transferred from the catalytic reactor to the surface analysis chamber. In particular, the catalyst surface should not be exposed to any atmosphere other than that similar to the one under which the reaction was performed. This usually poses a problem since photoelectron spectroscopic techniques, including XPS and AES, require ultra high vacuum (UHV) conditions so as not to inhibit the mean free path of photoelectrons between the sample and electron analyser. Real *in situ* testing of the catalyst surface is thus not possible since the mean free path of electrons would be too small for them to be detected. The best approximation is to quench the state of the reacting surface by rapidly exposing the working catalyst to UHV [38]. This may be achieved by installing a high pressure catalytic reactor either inside [39], or outside [40-42] the UHV analysis chamber. For the purpose of studying heterogeneous catalysis the latter option seems to be the more favourable one since it is technically less complicated and working atmospheres would not be as restricted [38]. The work described here was carried out using an external high pressure reactor linked to a UHV surface analysis chamber, via a sample transfer system, incorporating suitable pumping and valving arrangements. This enabled sequential reaction and surface analysis experiments to be carried out over the F-T catalysts. Coupled to the reactor is an on-line gas chromatograph for the detection and analysis of hydrocarbon products. Correlations between observed products as well as product distributions and the catalyst surface composition are thus facilitated.

2.2. Equipment

The equipment used has been extensively reviewed [42][43].

2.2.1. The combined high pressure reactor - surface analysis system

A Vacuum Generators (VG) "Solar 300" surface analysis UHV chamber constructed chiefly of mu-metal is the central feature. This is pumped by an Edwards EO4 oil diffusion pump and liquid nitrogen cold trap both with water cooled baffles. Additional pumping is provided by a VG titanium sublimation pump and Varian ion pump which separately pumps the X-ray source. A base pressure of approximately 4 x 10^{-10} mbar is obtainable. A VG "CLAM 100" system consisting of an X-ray source with Mg/Al dual anode for XPS, as well as an LEG61 electron gun for AES, is attached to the UHV chamber. (See Figure 2.1). Also attached to the UHV chamber is a VG AG2 ion gun. The x-ray and electron sources share the same detector which is a 150° spherical sector electron analyser with a channeltron detector. The sample for photoelectron spectroscopic analysis is vertically mounted to a high precision (manually operated) manipulator or translator. The translator has XYZ movement along with a full 360° rotation about the Z direction. In addition to this the manipulator has an azimuthal rotation of 180° around the centre of the sample along with a tilt mechanism which moves away from Z.

The external HPZ 10 high pressure reaction chamber, capable of withstanding pressures up to about 15 bar is linked to the UHV chamber via a Leybold-Heraeus VLP 10/63 introduction chamber. (See Figure 2.2). This chamber is in turn pumped by a turbomolecular pump attached to the roof of the chamber and base pressures of 5 x 10^{-9} mbar are obtainable. The introduction chamber is separated from the UHV chamber by a viton-sealed gate valve. A cylindrical rod with a cavity in which the sample is held is driven horizontally by a mechanized rod drive. Movement of the catalyst sample from the reaction chamber to the introduction chamber is via a short section of differentially pumped viton O-rings which seal directly onto the sample rod.

Catalyst discs were mounted onto a specially designed sample holder consisting of a rectangular molybdenum metal sheet with an area of 12 x 17 mm. The metal sheet is bent to form a U-shaped girder and relatively large end pieces are attached to it in order to provide mechanical strength. Gold or molybdenum clips fastened by means of screws were used to secure the catalyst discs to the front of the sample holder. (See Figure 2.3).

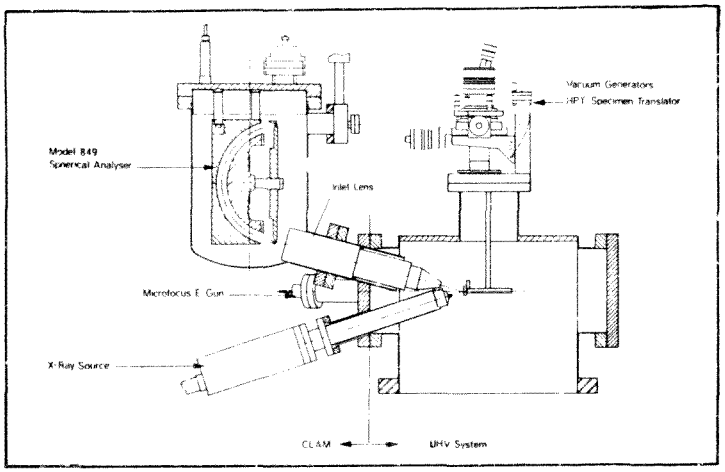

Figure 2.1. Schematic of the "CLAM 100" system attached to the "Solar 300" UHV chamber.

The sample and holder fits "face down" into the recess in the sample transfer rod and is held there by means of three copper conductors of which one can move 2mm along the axis of the rod via a manually operated spring loaded cam drive. Treatments are administered with the catalyst "face down" within the rod's recess in the reaction chamber. Temperatures for the various treatments are controlled and administered by means of passing AC current through the sample via the copper conductors in the rod. The treatment temperature is monitored by a chromel-alumel thermocouple which is screwed vertically down through a valve (see Figure 2.4) into

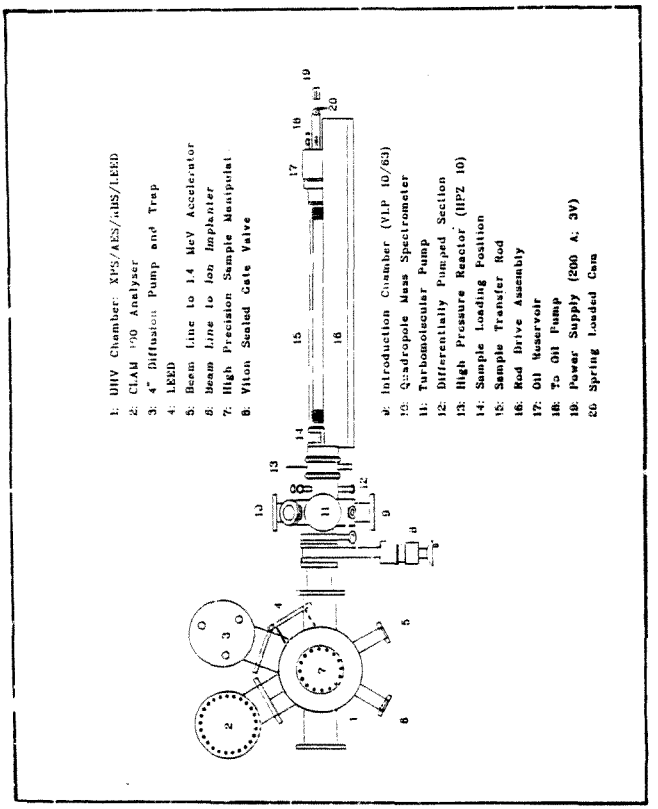

Figure 2.2. Schematic of the high pressure reactor (or HPR) - UHV system.

the reaction chamber to touch the back of the sample holder (now the molybdenum heater). To ensure that temperature measurements could be made without making electrical contact between the thermocouple and sample holder, a diamond (because of

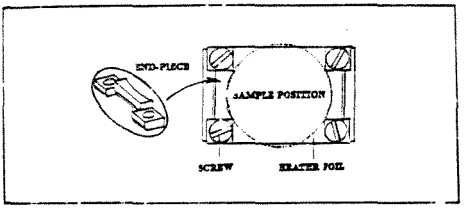

Figure 2.3. The transferable sample holder (viewed "face up").

diamond's excellent heat conduction and very high electrical resistance), was attached to the tip of the thermocouple [44] as in Figure 2.4. With prolonged use however, the diamond became dislodged, and so for subsequent reaction sequences a flat diamond with a large surface area was attached to the back of the sample holder [45]. In both cases, the diamond was attached by means of brazing to the metal using a gold-based eutectic brazing alloy.

Temperature measurement deviations

Measured temperatures have been shown to be dependant on the degree of contact between the sample and sample holder. After certain treatments, the change in surface characteristics could only be explained if it was assumed that the actual treatment temperature was lower than the one measured experimentally. On examination of the current and voltage values across the sample holder, where such cases occurred, it was found that the applied currents and voltages were lower than for the other treatments where the "same" temperature was measured. Since the thermocouple in effect measures the temperature of the sample holder, this implies that thermal contact between the sample and sample holder was not as efficient as for the other treatments.

2.2.2. The gas handling system

The gas handling system which incorporates purification traps, pressure regulation, flow meter control as well as an on line gas chromatograph (or GC), is directly linked

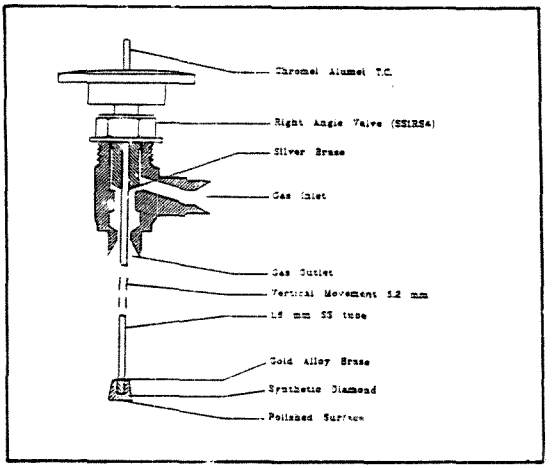

Figure 2.4. Schematic of the thermocouple used to monitor sample treatment temperatures in the HPR.

to the high pressure reactor. (See Figure 2.5). The arrangement of this equipment has been discussed in much detail [43].

A Shimadzu 14A gas chromatograph with FID and TCD detectors was used to analyse hydrocarbon-containing gases that had passed over the catalyst in the reactor. 2 ml volumes of product containing gas (tail gas) from the reactor were injected directly into the FID column of the GC for hydrocarbon separation via a sample loop. The stainless steel tubing between the reactor and GC, through which the tail gas flows, was heated to approximately 120 °C by nichrome resistance wire so as to prevent condensation of the gaseous hydrocarbon products.

Key to Figure 2.5. (On following page)

1, 2, 3. Gas lines.

4. Needle valve.

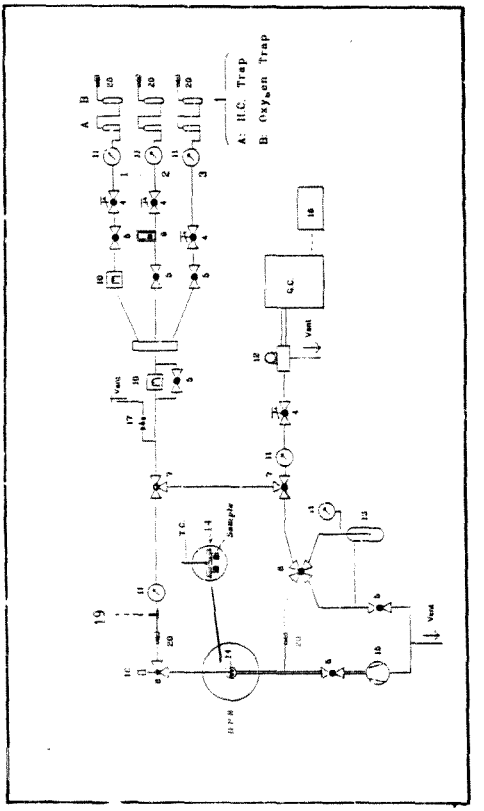

Figure 2.5. Schematic of the gas handling system coupled to the high pressure reactor. (See following and preceding pages for a key to various components in the schematic).

5. Two-way shut off valve.

6. Right angle valve.

7. Two-way valves.

8. Four-way valve.

9. Rotameter (for measuring high flowrates, typically 1350 ml/min.).

10. Mass flow meter (measures slow flowrates, typically less than 10 ml/min.).

11. Pressure guages.

12. Sample loop to gas chromatograph.

13. Hydrocarbon trap (not used).

14. Sample ("face down") in sample holder.

15. Rotary pump.

16. GC detector output integrator.

17. Pressure release valve.

18. "Go" pressure regulator.

19. Removable septum for injection of gases during catalyst poisoning experiments.

20. Quick-connects to gas cylinders and the high pressure reactor.

2.3. Experimental conditions

Variations in experimental treatment procedures and specific treatment sequences are outlined at the beginning of each of the subsequent chapters where results are given and discussed.

2.3.1 Sample preparation

Cobalt-manganese oxide catalysts with a Co/(Co + Mn) atomic ratio of between 0.45 and 0.50 were used. The catalyst preparation has been reported elsewhere [46] [47] and involves co-precipitation from cobalt and manganese nitrates at 70°C and a constant pH of 8.3 (according to guidlines first laid down by Maiti *et al.* [48]). Potassium promotion of the cobalt manganese oxide was achieved using the incipient wetness technique and co-precipitation of the cobalt and manganese salts in the presence of potassium carbonate [49]. Precipitation was followed by washing of the samples (with distilled water), drying and calcining at 500°C for 24 hours. Uncalcined catalyst samples give variable activities, and calcining has been shown to overcome this problem [50]. Calcining was followed by pressing a fixed mass of the catalyst powder into discs with a diameter of 8 mm which were 2 mm thick using a standard 15 ton press.

Preparation of the industrial iron catalyst samples is reported elsewhere [43] [51]. Briefly, samples were cut from fused lumps of magnetite to which a number of promoters had been added (see Chapter 5). A hollow diamond tipped drill was used to cut cylinders out of the fused material, from which discs (of the same size as the Co/MnO discs) where cut using a slow speed diamond saw. Polishing of the discs with water paper and alumina powder then followed before cleaning in an ultrasonic bath with AR acetone.

All samples were attached to the molybdenum sample holder (see Figure 2.3) before being loaded into the sample rod and transfered to the combined HPR-UHV system for treatments and analyses.

2.3.2. Sample treatment conditions

For all the experiments, high purity gases were used. (Argon (99.999%), H_2 (Afrox UHP 99.999%), CO (99.9), in H_2 /CO mixtures UHP H_2 was used along with 99.9% pure CO).

Apart from the reduction experiments performed on pure Co/MnO, all subsequent H_2 treatments were administered using a measured temperature of 400°C and a pressure of 500 kPa.

For the CO-hydrogenation studies over Co/MnO with and without potassium promotion, the CO-hydrogenation treatments were administered using a measured temperature of 190°C and a pressure of 500 kPa. These conditions were selected using kinetic and reactor study data generated by van der Riet *et al.* [47]. The F-T or CO hydrogenation reactions were carried out using synthesis gas with a H_2 :CO ratio of 20:1, along with high flowrates (in the order of 500 ml.min^{-1}) over the sample.

The conditions for monitoring the effect of H_2S poisoning on the synthesis activity of the industrial iron catalyst were the same as those employed in previous F-T studies on the catalyst [43]. It was also decided that sulphur injection or poisoning at low temperature would be a good starting point in the event of such poisoning studies being followed through more extensively [52]. CO-hydrogenation reactions over the iron catalyst were thus performed at 240°C using a pressure of 600 kPa, a flowrate of 600 ml.min^{-1} and synthesis gas with a H_2 :CO ratio of 20:1. Between F-T treatments, 2 ml H_2S injections were administered at room temperature and with the pressure in the reactor being 100 kPa whilst the catalyst was in a pure H_2 atmosphere. In order to administer the H_2S, an air tight septum was fitted near the reactor inlet (see Figure 2.5).

With both catalysts, the high flowrates and high H_2 :CO ratios were used to prevent excessive build up of carbonaceous material on the catalysts which in turn would make surface analysis difficult in the sense that carbon would mask the other elements thereby making it difficult to analyse them using XPS, but more importantly, to prevent excessive outgassing in UHV.

2.3.3. Data collection conditions

Reactor products

The gas chromatograph's FID detector was used to analyse the hydrocarbons produced by the CO-hydrogenation treatments.

A Porapak N (50/80) mesh column of length 2.2 m with helium carrier gas flowing through at a rate of 35 ml.min^{-1} was used. The column temperature was programmed to increase as follows:

Initial temperature : 38°C .

Final temperature 1 : 120°C .

Final temperature 2 : 140°C .

Rate of temperature increase : 10°C .min^{-1}.

Injection port temperature : 190°C .

Detector port temperature : 190°C .

Operating under these conditions, the GC could separate C_1 to C_6 hydrocarbons. Figure 2.6 shows a typical GC trace recorded at 6 hours F-T synthesis over a potassium promoted Co/MnO sample.

Connected to the GC was a Spectra Physics SP 4290 integrator which allowed quantification of output peak areas. (An integrator attenuation of 1 was used for all the experiments).

Surface analyses

An Al (Kα) X-ray source ($h\nu$ = 1486.6 eV[†]) was used for XPS. X-ray photoelectrons were generated using a positive potential of 11 keV, an emission current of 20 mA and analyser pass energies of between 20 and 100 eV.

Hardcopies of X-ray photoelectron spectra were obtained by means of a standard X-Y plotter directly attached to the spectrometer control unit. Data could be displayed as a function of kinetic energy on an IBM XT microcomputer screen and stored for further analysis.

AES spot analyses were performed between chemical treatments over the iron catalyst. Auger photoelectron spectra were collected using an acceleration voltage of 2.5 keV, a filament current of 2.5 A, a beam current of 10 μA, a pass energy of 200 eV and a spatial resolution of around 30 μm. (AES spectra are quoted in the conventional differentiated form).

[†]throughout this dissertation : 1 eV $\simeq$ 1.6 x 10^{-19} Joules.

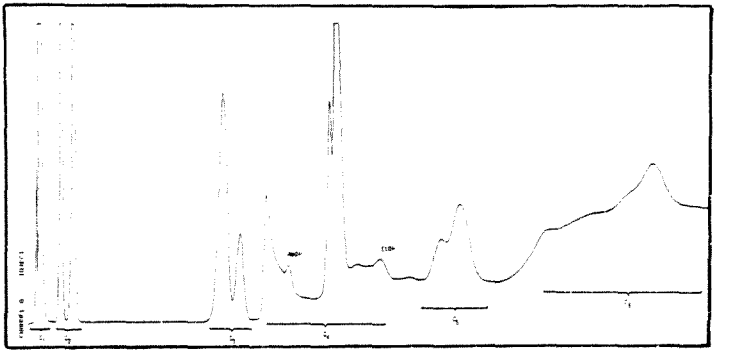

Figure 2.6. A typical GC trace after 6 hours F-T synthesis over a potassium-promoted Co/MnO catalyst.

The base pressure in the UHV chamber during XPS and AES analyses was always between 5 x 10^{-8} and 1 x 10^{-9} mbar.

2.4. Handling of data

Gas chromatograph data

Quantitative GC data was generated from the integrated FID responses. The area count of each component detected was multiplied by a correction factor that took the varying detector response for each component into account [53]. This allowed each hydrocarbon component's concentration to be calculated in terms of mass percent. All GC data has been quoted in terms of mass/mass percent ratios (or M/M %).

The identification of various hydrocarbon components was facilitated by comparing

peak positions with those generated after injection of standards using the same column conditions.

Photoelectron data

During surface analyses of the cobalt-manganese oxide catalysts, significant "charging" of the sample was observed even though the sample being analysed was earthed. This resulted in the e XPS spectra being recorded at a higher binding energy (or lower kinetic energy). Copperthwaite *et al.* [54] have observed substantial temperature dependant kinetic energy shifts (of around 5 eV) when recording XPS spectra collected from an iron-manganese oxide catalyst using the same equipment as that used in these studies. Such charging can be said to be due to the "p-type" semiconductor behaviour of MnO [54], which causes an increase in electical conductivity at high temperatures [55]. The same can be said of the Co/MnO catalysts studied in that increasing the temperature at which the XPS spectra were recorded was shown to increase the kinetic energy at which the various peaks were detected. Recording the spectra at higher temperatures was however not undertaken since doing so may have caused changes at the catalyst surfaces. For these reasons, catalyst charging was corrected for using an oxygen or O (1s) photoelectron signal with a binding energy (or BE) of 530.0 eV as a reference [54]. The reason for choosing the O (1s) signal as a reference is that this signal remained fairly constant under all conditions, and the oxide O^{2-} was always the most abundant component at the surface. Charging of the iron catalyst was corrected for using the potassium K ($2p_{3/2}$) signal with a binding energy of 293.6 eV $\pm$ 0.3 eV [56].

Computer fitting of up to three Gaussian peaks to the raw data using a micromin least squares fitting routine facilitated the determination of peak areas and subsequent quantification of the XPS data. A more detailed discussion of the computer simulated peak fitting procedures is outlined elsewhere [43].

Due to the fact that Co/MnO catalysts were used in the form of compressed discs of powder, it is difficult to apply XPS quantification procedures with a great deal of accuracy. A knowledge of the sample density and it's exact chemical composition is required before photoelectron escape depths can be calculated, and quantification can be performed. This is true for the well known Madey - Yates [57] equation and its' adaptations [58], as well as for the formulae published by Seah *et al.* in 1979 [59]. These

formulae all include monolayer calculations which would be irrelevant to the Co/MnO study since the catalyst surfaces were unpolished and presumably highly amorphous as well as porous.

Calculation of photoelectron escape depths for these catalysts are further complicated by the segregation of various components in the solid during treatments. This results in compositional changes, including density changes that could not be measured using our equipment.

Penn [60] has shown that relative surface concentrations of different atoms in an alloy, say for simplicity, type 1 and type 2 atoms can be given by the equation

$$\frac{\eta_1}{\eta_2} = \frac{I_1}{I_2}\frac{\sigma_2}{\sigma_1}\frac{D(\varepsilon_2)}{D(\varepsilon_1)}\frac{\lambda_T(\varepsilon_2)}{\lambda_T(\varepsilon_1)} \tag{1}$$

where η_1/η_2 is the relative concentration of type 1 and type 2 atoms, I_1/I_2 is the relative signal strength observed by XPS measurements, σ is the photoionization probability (as calculated by Schofield [61]), D is the fraction of electrons detected by the analyser and $\lambda_T(\varepsilon_2)/\lambda_T(\varepsilon_1)$ is the ratio of the mean free paths of photoelectrons with energy ε_1 and ε_2 coming from type 1 and type 2 atoms in the alloy. This electron escape depth ratio can be shown to be approximated by equation (2).

$$\frac{\lambda_T(\varepsilon_2)}{\lambda_T(\varepsilon_1)} = (\frac{\varepsilon_2}{\varepsilon_1})[(ln\ \varepsilon_1 - 2.3)/(ln\ \varepsilon_2 - 2.3)] \tag{2}$$

This expression can be used directly in equation (1), which in turn can easily be modified to facilitate relative surface atomic percentage (herewith abbreviated as r s.a.p.) calculations for more than two elements.

Furthermore, Penn states that to a fairly good approximation there is a material independant behavior of $\lambda_T(\varepsilon_2)/\lambda_T(\varepsilon_1)$ as a function of ε_2 and ε_1 for $\varepsilon_1, \varepsilon_2 \geq 200$ eV [61]. The use of equation (2) for the calculation of photoelectron escape depths can be shown to result in at most, an error of 14% but more typically, one in the region of 5% is incurred.

For the purposes of this study, relative atomic percentages of elements at the surface or near surface were calculated. These values were obtained using Penn's formulae as a basis.

In instruments where the analyser energy is fixed, such as the one used in this study, the transmission is inversely proportional to the kinetic energy of the electrons, hence the D's in equation (1) can be replaced by values of $1/E_K$. Since the photoionization probability is directly proportional to the core level photoionization cross section (PIC) of an element, a PIC for each element can be substituted into equation (1) as that elements' σ value. A value of $\lambda_T(\varepsilon)$ for each element was calculated using equation (3). (See Table 2.1).

$$\lambda_T(\varepsilon_1) = \frac{\varepsilon_1}{(ln\ \varepsilon_1 - 2.3)} \tag{3}$$

Where $\varepsilon_1 = E_K$ for photoelectrons from element 1. Surface concentration values for each element were then obtained from the equation (4).

$$\eta_1 = \frac{A_1 S_1 E_{K1}}{\sigma_1 \lambda_T(E_{K1})} \tag{4}$$

A_1 is the integrated XPS signal area/s and S_1 is the detector sensitivity setting for an element. (In this case, element 1).

Arbitrary values for the total surface concentrations were obtained by adding the η values of detected elements,

$$\eta_{total} = \eta_1 + \eta_2 + \eta_3 + \cdots \eta_i \tag{5}$$

and the relative surface atomic percentage ($r.s.a.p$) of each element (for example, element 1) calculated using equation (6).

$$r.s.a.p._1 = \frac{\eta_1}{\eta_{total}} 100\% \tag{6}$$

The AES data collected from the industrial iron catalyst was analysed qualitively. Quantification of the AES data was difficult since signal sensitivities changed according to changes in the sample/beam geometries and the amorphous and rough catalyst surface (especially after the various treatments). For these reasons, comparisons of peak heights of different elements in the same scan were made.

Element	λ_T
Carbon	250.9
Potassium	294.4
Oxygen	210.0
Manganese	190.3
Cobalt	166.0

Table 2.1. λ_T values calculated for carbon, potassium, oxygen, manganese and cobalt.

Chapter 3. Reduction and carburisation of cobalt-manganese oxide

3.1. Experimental route

The catalyst preparation has been reported elsewere [47]. A calcined Co/Mn_xO catalyst with a Co/(Co + Mn) ratio = 0.455 was used. The catalyst surface was analysed by XPS between treatments in the high pressure reactor (HPR) in the following sequence:

1. Before treatment.
2. After H_2 at 260°C (12 hours).
3. After H_2 at 360°C (6 hours).
4. After H_2 at 400°C (6 hours).
5. After CO at 220°C (25 minutes).
6. After CO at 280°C (18 minutes)
7. After Ar^+ bombardment (8 kV beam energy for 10 minutes)

All the reactions were carried out using using flowrates of ± 20 cc per minute and at 500 kPa using high purity gases (see experimental chapter). The final treatment, which involves bombarding the sample with argon ions, was performed in order to remove surface layers and facilitate examination of the sub-surface or bulk composition. This was performed using a VG AG2 ion gun.

3.2. Results and discussion

The text refers to the C (1s), O (1s), Mn ($2p_{3/2}$) and Co ($2p_{3/2}$) XPS spectra recorded between the various treatments. These figures, as well as tables and graphs which illustrate the quantified data are shown at the end of this chapter. The r.s.a.p.'s of the elements detected at the surface between the various treatments are quoted in Table 3.1.

3.2.1 Untreated catalyst

Before the catalyst was treated in the HPR, the C (1s) peak is seen to have a BE of 285.1 eV, and this is assigned to hydrocarbon contamination. C (1s) signals around 285.0 eV are commonly refered to as "adventitious" carbon and are often used as references to correct for sample charging [54][62].

The quantified data shows that there is significantly more manganese at the surface with respect to cobalt, in that the Co/Mn ratio is 0.59 compared with a bulk Co/Mn ratio of approximately 1. Baerns *et al.* [62] have studied the surfaces of calcined and reduced Fe/MnO catalysts by XPS, using catalyst samples prepared similarly to the Co/MnO catalysts used for this study. Although calcination of their Fe/MnO samples was carried out under an argon atmosphere (also at 500°C for 24 hours), their results also show that for catalysts with similar iron loadings to the cobalt loadings used in this work, there is significant enrichment of manganese at the surface with respect to iron. X-ray diffraction studies of Co/MnO catalysts [50] show that calcination increases the degree of substitution of cobalt and manganese into octahedral and tetrahedral sites in the Co/MnO catalyst which, before calcination, is comprised of a range of cobalt-manganese spinels. These consist of a range of Co_2MnO_4 and $CoMn_2O_4$ type spinels where cobalt and manganese ions occupy exclusively either octahedral or tetrahedral sites, as well as a mixed spinel phase in which cobalt and manganese ions occupy octahedral and tetrahedral sites non exclusively.

The Mn ($2p_{3/2}$) signal has a BE of 642.0 eV and may be assigned to Mn^{3+} by virtue of the fact that no shake-up satellite is observed, since high spin electron configurations are expected to give rise to shake-up satellites, but Mn^{3+} has a low spin d^4 configuration. The high BE (642.0 eV) of the signal may however be indicative of Mn^{4+}. Allen *et al.* [63] have undertaken a XPS study of a number of mixed transition metal oxide spinels and show Mn ($2p_{3/2}$) photoelectron spectra of pure MnO_2, Mn_3O_4 and Mn_2O_3 with B.E's of 642.2, 641.7 and 641.8 eV respectively, none of which show any evidence of shake-up satellites. Included in their work is a Mn (3p) spectra of pure MnO in which no shake-up satellite is observed. They have also shown that the Mn ($2p_{3/2}$) lineshape changes when manganese is included in spinel structures in that there are shake-up satellites when this is the case. Spectra of pure MnO supports which have been covered

with iron show a definite shake-up satellite at the high BE side of the main Mn ($2p_{3/2}$) photoelectron peak [54].

The Co ($2p_{3/2}$) signal with a BE of 780.7 eV is assigned to Co^{2+} from Co_3O_4 and/or CoO. This is confirmed by the weak shake-up satellite at the high BE side of the main peak indicating that a high spin d^7 configuration for the cobalt is most likely. Larkins *et al.* [64] have studied the surface of pure Co_3O_4 using XPS and found an asymmetric Co ($2p_{3/2}$) peak with a maximum at 779.5 eV. These workers showed that heating their sample gave rise to a larger signal at 781.0 eV associated with paramagnetic Co^{2+}. The Co ($2p_{3/2}$) BE of Co^{2+} was shown to be higher than that of Co^{3+} which is opposite to the result normally expected. This is believed to be due to the fact that the Co^{2+} ions occupy tetrahedral sites in a high spin configuration, with a larger number of close neighbours than Co^{3+} in the octahedral sites.

The large proportion of oxygen at the surface is associated with O^{2-} ions from the cobalt and manganese oxides at the expected O (1s) BE of 530.0 eV [54].

3.2.2. Reduction (or H_2) treatments

After the reduction treatments at 260°C and 360°C, the C (1s) signals shift to a lower BE of 284.3 eV, and this is assigned to carbon being primarily of a graphitic nature, with a large portion being carbide. This is illustrated by the shoulders on the low BE sides of the main C (1s) signals. BE's for the XPS determination of graphite and carbide are most commonly quoted as being at 284.4 and 283.3 eV respectively [65]. After the H_2 treatment administered at 260°C the r.s.a.p. of carbon increases from 7.7% to 11.3%, indicating that there is surface segregation of carbon impurities from the catalyst bulk. Reduction at 360°C shows that further segregation of carbon takes place since the r.s.a.p. of the carbon is seen to increase to 13.2%. By increasing the reduction temperature to 400°C, the surface carbon is hydrogenated away, presumably as methane.

During reduction treatments, the Mn ($2p_{3/2}$) peaks are seen to shift to a lower BE of 640.6 eV, and there are discernable though small changes with regard to the appearance of shake-up satellites at 647.1 eV. The Mn ($2p_{3/2}$) signals do however become broader, and this may be due to the manganese having more than one oxidation state. This

broadening could also contribute to obscuring of the shakeup satellites one would expect to be associated with BE's for Mn ($2p_{3/2}$) signals at 640.8 eV.

The surface cobalt is seemingly unaffected by the H_2 treatment administered at 260°C , but becomes reduced at 360°C and remains so at 400°C . This is illustrated by the chemical shift of the Co ($2p_{3/2}$) peak from 780.5 to 778.1 eV after reduction at 360°C . The Co ($2p_{3/2}$) peak at 778.1 eV is in agreement with reported values for clean Co metal [66-68]. The observed transition to metallic cobalt is further highlighted by the disappearance of the shake-up satellite associated with high spin d^7 Co^{2+}. The H_2 treatment at 260°C leads to a decrease in the Co/Mn ratio from 0.5 to 0.44. This difference may however not be significant, since an error of up to 14% (but more commonly one of 5%) has been allowed for in calculations of the various element concentrations at the surface. On reduction at 360°C and 400°C , there is a very significant decrease in the Co/Mn surface ratio (from 0.44 to 0.12), indicating high enrichment of manganese with respect to cobalt at the surface.

Baerns *et al.* have shown that there is significant enrichment of manganese with respect to iron after reduction of Fe/MnO catalysts, and have put forward a theory on how this takes place based on comprehensive bulk and surface studies of the catalyst, all performed under similar conditions [62][69-72], as well as results obtained from Engell *et al.* [73][74] and Schmalzried [75] who investigated the reduction of mixed Fe_3O_4-Mn_3O_4 oxides. These workers claim evidence for reduction starting in the bulk and not at the oxide surfaces, and that reduction of FeO-MnO results in the depletion of iron at the surface because metallic iron diffuses to the nearest precipitation point. Vacancies are then filled with manganese which was stated to have a very high diffusivity in MnO and could therefore diffuse over large distances.

X-ray diffraction studies of calcined Co/MnO samples [50] after they had been reduced indicated that the mixed spinel $(Co,Mn)(Co,Mn)_2O_4$ is the dominant phase. These bulk studies have also shown that the reduced catalyst contains significant quantities of Co metal and MnO.

The fact that the r.s.a.p. of oxygen decreases after the 360°C H_2 treatment may be ascribed to the large decrease in the cobalt which was shown to be in the form of CoO or Co_3O_4 prior to increasing the reduction temperature. The decrease in oxygen at the surface is therefore linked to an increase in as well as reduction to metallic cobalt. (Later

studies show that there is a relationship between carbon and oxygen at the surface, and that when the concentration of one increases, the concentration of the other decreases). A broadening of the O (1s) signal at the low BE side is seen to be brought about by the H_2 treatments and this may be associated with the the broader Mn ($2p_{3/2}$) signals, which indicate the presence of more than one oxidation state for manganese.

3.2.3. Carburisation (or CO) treatments

After pure CO is administered to the Co/MnO catalyst, there are two types of carbon species left at the surface. These species give rise to C (1s) signals with BE's of 284.3 and 289.6 eV. These two peaks have been assigned to graphitic and chemisorbed CO_2 respectively. A carbon (1s) peak with a BE of ± 290 eV assigned to a carbonate species has been detected on a reduced industrial iron catalyst after exposure to atmosphere [43]. Upon increasing the temperature at which the catalyst is exposed to CO, the area of the peak with the higher BE is seen to decrease, whilst the C (1s) peak assigned to graphite increases. The fact that the graphitic signal increases whilst the signal at 289.6 eV decreases, may be taken as evidence that the high BE signal is due to a $CO_{2(ads)}$ species, since these species are known to desorb with increasing temperature. Furthermore, graphite is known to be stable over cobalt surfaces [76].

Carbon deposited at the surface increases from 12.5% to 20.1% when the CO treatment temperature is increased from 220°C to 280°C . An increase in the r.s.a.p. of carbon (or more specifically, graphite) would be expected if a chemisorbed CO or carbonyl was dissociating. CO adsorption studies of iron supported on MnO [54] report a C (1s) BE of 287.0 eV (± 0.3 eV) as $CO_{(ads)}$ which has a significantly lower C (1s) BE compared with the value of 289.6 eV obtained with the Co/MnO catalyst. This may be taken as negative evidence for the the observation of adsorbed carbonyl species over cobalt-manganese oxide in this study.

Bonzel *et al.* have however assigned a C (1s) BE of 285.7 eV to molecular CO on cobalt [76] (The experiments, using pure CO over a metallic cobalt film were performed at 325°C). These workers claim that by increasing the temperature, molecular CO forms exclusively carbide (C (1s) BE at 283.4 eV). Similar studies to those discussed in this chapter using pure CO over reduced industrial catalysts [43] show that a high build-up of carbon occurs at around 150°C and that iron carbide is converted to graphitic

carbon which would result in the catalyst having a lower F-T or CO-hydrogenation activity. Graphitic carbon build-up is known to reduce the rate of hydrocarbon synthesis and act as a partial poison over metallic iron surfaces [77]. Carbon build-up over the industrial iron catalysts was far more pronounced after the pure CO treatments compared with the cobalt-manganese oxide used in this study, and this may contribute towards explaining the longer lifetimes obtained with the Co/MnO catalysts observed under F-T conditions.

The Mn ($2p_{3/2}$) signals sharpen considerably when pure CO is passed over the catalyst at 220°C and 280°C , indicating that probably only one form of manganese is at the surface. The BE's are seen to move to a slightly higher value for both CO treatments (although this shift may not be significant since an error of ± 0.3 eV is allowed for). Furthermore, shake-up satellites appear. The combination of these factors indicate that Mn^{2+} is the predominant form of manganese at the surface. The apparent increase in the Mn ($2p_{3/2}$) BE associated with a transition from Mn^{3+} to Mn^{2+} may be explained by the previously mentioned argument put forward by Larkins *et al.* for interpretation of Co ($2p_{3/2}$) peaks, if the Mn^{2+} and Mn^{3+} occupy tetrahedral and octahedral sites respectively.

The O (1s) spectra after CO treatments are also seen to become narrower, and this corresponds to what is observed with the Mn ($2p_{3/2}$) spectra after the CO treatments.

Furthermore, the reduction of manganese at the surface to MnO may be linked to the appearance of the $CO_{2\,(ads)}$ species after the CO treatments by the following reactions:

$$CO_{(g)} + O^{2-}_{(s)} \longrightarrow CO_{2\,(ads)} + 2e^-$$

$$2Mn^{3+}_{(s)} + 2e^- \longrightarrow 2Mn^{2+}_{(s)}$$

$$O^{2-}_{(s)} + CO_{(g)} + 2Mn^{3+}_{(s)} \longrightarrow CO_{2(ads)} + 2Mn^{2+}_{(s)}$$

Re-oxidation of the cobalt is seen to take place when pure CO is passed over the sample at 220 and 280°C . This is indicated by the BE shift from 778.1 to 780.6 eV and the appearance of shake-up satellites, again associated with high spin (d^7) Co^{2+}. Re-oxidation of the cobalt is associated with an increase in the Co/Mn ratio at the surface

from 0.12 after the H_2 treatment at 400°C , to 0.31 and 0.30 after pure CO treatments at 220 and 280°C respectively. This re-oxidation phenomenon was not observed when synthesis gas was passed over reduced *Co/MnO catalysts* in later studies (although it should be noted that 5% CO in H_2 gas mixtures were used).

The re-oxidation of the cobalt during the CO treatments may be linked to the reduction of the manganese which could result in the liberation of oxygen or oxide ions over the catalyst. It is however, more likely that cobalt re-oxidation is associated with the observed buildup of "inert" carbon (with a C (1s) BE of 284.3 eV) caused by the pure CO treatments. This may be facilitated by the following reactions at the surface:

$$CO_{(g)} + 2e^- \longrightarrow {}'C^{o}{}''_{(s)} + O^{2-}_{(s)}$$
$$Co_{(s)} \longrightarrow Co^{2+}_{(s)} + 2e^-$$
$$\overline{Co_{(s)} + CO_{(g)} \longrightarrow CoO_{(s)} + C_{(s)}}$$

The apparently opposing effects of H_2 and CO treatments with respect to reduction and oxidation of cobalt and manganese suggests that electronic effects may have some influence on the mechanism of hydrocarbon formation over these catalysts. The increase in the Co/Mn ratio at the surface after the CO treatments may be linked to the re-oxidation of the cobalt if the previously discussed reduction model [73-75], can be extrapolated to Co/MnO catalyst systems. The idea being that since cobalt was being oxidised, metallic cobalt would no longer diffuse to the nearest precipitation point.

3.2.4. Argon ion bombardment

Argon ion (Ar^+) bombardment or sputtering was performed in order to ascertain possible differences between the sample surface and bulk.

This treatment reveals that the catalyst bulk contains carbon, which by virtue of the C (1s) BE at 283.3 eV is assigned to carbide. The fact that carbide is observed after sputtering may indicate that a bulk carbide phase is stable for these catalyst systems, however the possible effect of ion beam modification of the surface should not be discounted. Bulk carbide phases in Fe/MnO catalysts have been reported

[69][78]. The carbon peak observed after the Ar^+ treatment may indicate that there was diffusion of carbon into the bulk during the CO treatments, or that there was bulk carbon contamination during sample preparation. The latter option is unlikely since the samples were prepared under rigid conditions and further studies on these catalyst systems show that surface segregation of bulk carbon takes place during reduction at temperatures around 400°C , and that no further carbon is observed after subsequent Ar^+ sputtering. Furthermore, no further segregation of carbon was observed when the reduction temperature was increased to 400°C . The r.s.a.p. of carbon after sputtering is 15.5% as compared to 20.1% after the final CO treatment, indicating that a large portion of the surface carbon migrates to the bulk of the catalyst, or that there is diffusion of CO into the catalyst bulk. It may also be expected that one, or both of these processes would occur since the Co/MnO samples were comprised of pressed discs of powder, and were therefore porous.

Ar^+ sputtering of the catalyst surface after treatment with CO at 280°C results in a decreased oxygen concentration (47.2% to 32.9%). This is associated with a manganese r.s.a.p. of 39.2%. Neither the O (1s) and Mn ($2p_{3/2}$) lineshapes are seen to change after Ar^+ bombardment. This, coupled to the similarity in the r.s.a.p.'s of oxygen and manganese, gives a good indication that the new surface's oxygen and manganese is virtually entirely comprised of MnO, since the Mn/O atomic ratio closely approximates a value of 1. Assuming minimal differential sputtering of the different elements, as well as minimal ion beam modification of the catalyst surface, it may be assumed that MnO is the predominant form of manganese in the bulk after the various treatments. The observed transition to metallic cobalt further explains the decrease in the amount of oxygen observed after Ar^+ bombardment.

The cobalt is metallic as indicated by the sharp Co ($2p_{3/2}$) peak with a BE of ± 778.2 eV. The shoulder around 780.6 eV is indicative of a small amount of oxidised cobalt, but it is tempting to associate this shoulder with a cobalt carbide species. Although the Co/Mn ratio of 0.32 is virtually unchanged with respect to the Co/Mn ratio after the CO treatment at 280°C , there is significantly more cobalt after sputtering (12.4% as compared with 7.1% before sputtering). This corresponds well with the assumption that reduced cobalt may migrate to the bulk, and/or that bulk reduction of cobalt occurs. Ar^+ bombardment of an untreated Co/MnO catalysts in the following

chapter using similar conditions shows that the employed sputtering conditions do not bring about reduction of the cobalt.

3.3. Conclusions

From the results, cobalt is shown to become reduced more easily with H_2 than is manganese, and both the calcined and reduced catalysts have a cobalt to manganese surface composition which is different from that of the bulk. There is a very significant depletion of cobalt at the surface after reduction, and metallic cobalt is observed after argon ion bombardment or surface etching. These observations may be explained by the model of "inner reduction" as suggested by Engell and Schmalzried. Treatments with pure CO have the effect of re-oxidising the metallic cobalt to CoO and reducing all the manganese to MnO.

There is evidence for a carbon species with a high binding energy C (1s) XPS signal assigned to $CO_{2\ (ads)}$ on MnO. The stability of this species (as expected) is sensitive to changes in temperature, in that there is more adsorbed CO_2 when pure CO was administered at lower temperature. This $CO_{2\ (ads)}$ species may, or may not take part in the hydrocarbon chain formation prior to desorbing and/or dissociating, and these possibilities will be discussed in the following chapter.

Graphite formation is observed at the surface, and carbide formation takes place in the catalyst bulk. Carbon build-up however, is less marked over the Co/MnO system when compared with Fe/MnO and industrial iron catalysts.

3.4. Data collected for the reduction and carburisation study over a cobalt-manganese oxide catalyst

See following pages.

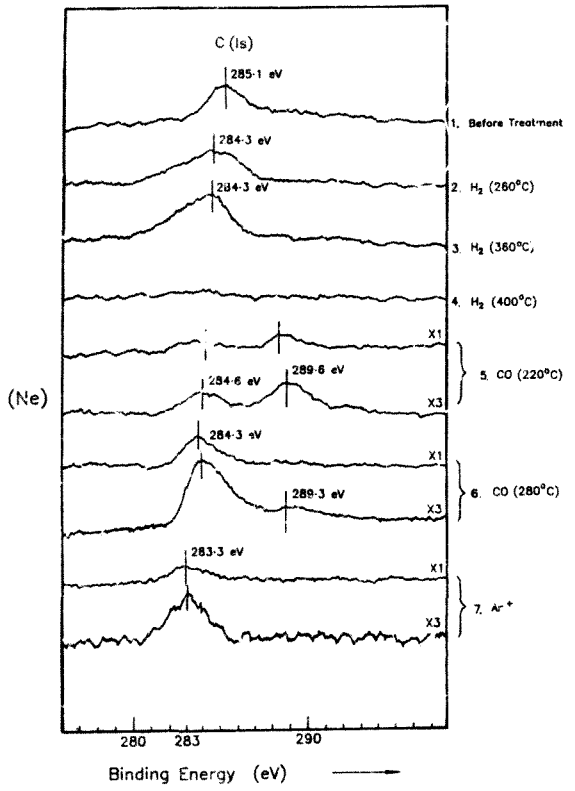

Figure 3.1. XPS spectra recorded in the C (1s) region between various treatments, for the reduction and carburisation study with Co/MnO.

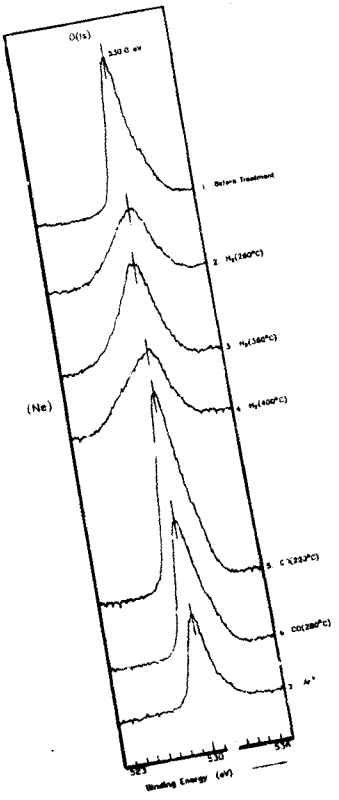

Figure 3.2. XPS spectra recorded in the O (1s) region between various treatments, for the reduction and carburisation study with Co/MnO.

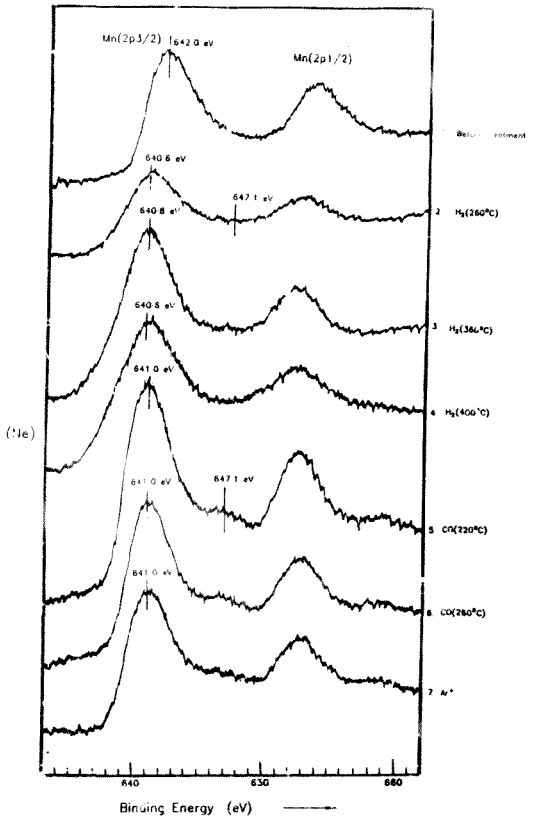

Figure 3.3. XPS spectra recorded in the Mn ($2p_{3/2}$) region between various treatments, for the reduction and carburisation study with Co/MnO.

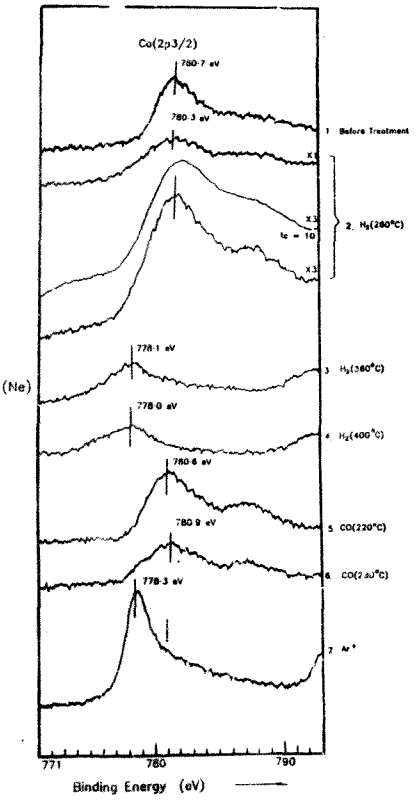

Figure 3.4. XPS spectra recorded in the Co ($2p_{3/2}$) region between various treatments, for the reduction and carburisation study with Co/MnO.

	R.S.A.P.'s OF ELEMENTS BETWEEN TREATMENTS			
TREATMENT	C	O	Mn	Co
1	7.7	58.3	22.7	11.3
2	11.7	55.5	22.7	10.1
3	13.2	50.1	32.8	3.9
4	0.0	57.7	37.7	4.6
5	12.5	52.4	26.8	8.3
6	20.1	47.2	25.7	7.1
7	15.5	32.9	39.2	12.4

Table 3.1. Relative surface atomic percentages of elements between treatments, for the reduction and carburisation study with Co/MnO.

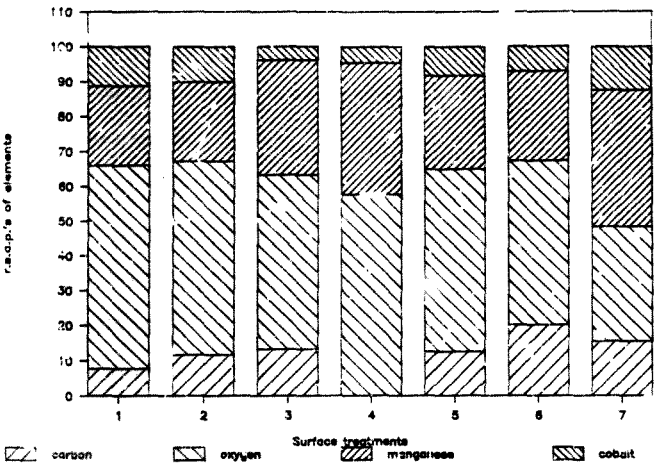

Figure 3.5. **Graphic illustration of relative surface atomic percentages of elements between t eatments for the reduction and carburisation study with Co/MnO.**

Chapter 4. CO-hydrogenation over cobalt-manganese oxide catalysts

4.1. Experimental route

Calcined Co/MnO catalysts with a Co/(Co + Mn) ratio of 0.48 were used.

Catalyst A was analysed by XPS in the following sequence:

1. Before treatment.
2. After Ar^+ (5 kV beam energy for 15 minutes).
3. After 6 hours H_2 at 400°C .
4. After 5 min. F-T synthesis.
5. After 15 min. F-T synthesis.
6. After 30 min. F-T synthesis.
7. After 1 hour F-T synthesis.
8. After 3 hours F-T synthesis.
9. After 6 hours F-T synthesis.
10. After 12 hours F-T synthesis.
11. After 24 hours F-T synthesis.
12. After Ar^+ bombardment (4.6 kV beam energy for 15 minutes).

The initial Ar^+ treatment was performed in order to "clean" the sample, whilst the final Ar^+ treatment (treatment number 12) was undertaken so as to ascertain possible differences between the catalyst surface and bulk characteristics (for catalyst A). The above treatment sequence was repeated on a Co/MnO catalyst (catalyst B) with exactly the same composition so as to establish reproducibility of results. In the second study the catalyst underwent a re-reduction with H_2 for 12 hours at 400°C after it had undergone a total of 24 hours F-T synthesis. This step was performed instead of Ar^+ bombardment.

4.2. Results and Discussion

The text refers to the C (1s), O (1s), Mn ($2p_{3/2}$) and Co ($2p_{3/2}$) XPS spectra recorded during the reaction sequence, and compares the results with those discussed in the previous chapter. The spectra, as well as tables and graphs, are shown at the end of this chapter. The r.s.a.p.'s of elements detected at the surface between the various treatments are quoted in Table 4.1

4.2.1. Untreated catalyst

Before treatments the catalyst surface was different to the sample used for the reduction and carburisation study in that there is significantly more carbon contamination on the catalyst to be used for the F-T synthesis study. (Compare Table 5.1 with Tables 3.1 and 4.1).

The O (1s) signal has a shoulder on the high BE side of the main photoelectron peak, and this is presumably due to the various metal oxides present at the surface before treatments are commenced. The Mn ($2p_{3/2}$) signal has it's major component at 642.2 eV. This is indicative of Mn^{4+} or MnO_2, as manganese in the 4+ oxidation state has a high spin d^3 electron configuration thereby giving rise to a shake-up satellite at a higher BE. This indeed is witnessed by the "hump" between the two photoelectron peaks.

The Co ($2p_{3/2}$) peak has a BE of 780.6 eV and their is a shake-up satellite between the main cobalt peaks, indicating the presence of Co^{2+} and not Co^{+3} (or a d^6 electron configuration).

4.2.2. Argon iron bombardment

As mentioned previously, Ar^+ bombardment was performed in order to ensure that the sample surface was "clean", and more specifically, to facilitate removal of the large amount of surface carbon contamination present.

After Ar^+ bombardment all the carbon is removed. This indicates that there was little or no bulk contamination of carbon in this catalyst. (Please refer to the previous discussion of reduction and carburization of a Co/MnO catalyst with respect to bulk carbide formation by CO treatments).

There is significant surface enrichment of manganese with respect to cobalt after the Ar^+ treatment. The Co/Mn surface ratio is 0.3 compared with a bulk ratio of approximately 1. The large increase in the r.s.a.p. of oxygen (50.6% to 74%) can be partially ascribed to the increase in manganese oxide(s). The increase in oxygen is however not proportional to the increase in manganese. The Mn/O ratio before treatment is 0.19 and this changes to 0.27 after argon ion bombardment. The reason for this may be expained by a number of factors.

Firstly, removal of the surface carbon, (of which a large portion was oxygenated) would contribute to a lower Mn/O ratio after bombardment.

Secondly, manganese is shown to be more reduced in the bulk, as illustrated by the $Mn(2p_{3/2})$ photoelectron peak shifting to a lower BE of 640.8 eV. This binding energy is usually associated with Mn^{2+} . The absence of a clear shake-up appears to be an anomaly. However, as mentioned previously, other researchers [63] have not observed shake-up satellites using XPS to study pure MnO samples, and this is presumably due to the presence of surface Mn_2O_3. The signal observed is probably caused by mixed oxides of manganese, including Mn_3O_4, and this would obscure a shake-up satellite.

Thirdly, the cobalt may have a slightly increased metallic character as indicated by the lower BE of 780.6 eV, and the broadened Co $(2p_{3/2})$ photoelectron peak, but as mentioned in the previous study, this peak may also be due to Co_3O_4.

Although ion beam modification of the surface may result in these changes, it is more likely that the catalyst bulk is not as oxidised as the surface. The removal of carbon contamination would be expected to result in an increase in the r.s.a.p.'s of the other elements. The fact that the Co/Mn ratio is lowered from 0.7 to 0.3 (approximately) after Ar^+ bombardment (and carbon removal) is again indicative that the amount of surface carbon plays a role in the Co/Mn ratio at the surface.

The changes between the surface and bulk cobalt and manganese are shown up in the O (1s) spectrum after the Ar^+ bombardment. The O (1s) signal is considerably broader with a shoulder at the low BE side of the main photoelectron signal, and sputtering with Ar^+ illustrates that the untreated catalyst bulk is less oxidised than the surface.

4.2.3. Reduction with H_2

After reduction of the catalyst for 6 hours with H_2 at 400°C , surface segregation of trace amounts of carbon from the bulk takes place. BE assignment to the C (1s) signal is difficult due to the broad photoelectron peak and the large signal to noise ratio because of the high sensitivity at which the spectrum was collected. In the previous reduction study, surface segregation of carbon was observed at 260°C and 360°C . This carbon was shown to be mainly graphitic in character with a considerable portion being carbide. (See Chapter 3, page 35).

Reduction of the catalyst has the effect of lowering the Co/Mn ratio from 0.3 to 0.16. The Co/Mn ratio of 0.16 corresponds well with values of 0.13 obtained after similar reduction treatments with the previous study and a mechanism by which this surface segregation takes has been discussed in the previous chapter.

The Mn ($2p_{3/2}$) signal is again a broad peak, and the BE is seen to shift to a slightly lower value. Although this shift is probably insignificant, it may be indicative that further reduction of some manganese has taken place. An excess of O^{2-} ions is known to be present in p-type MnO [55], and this is presumably responsible for the observed O/Mn atomic ratio value of approximately 2. As was the case in the previous study, the cobalt becomes reduced. This is shown by the shift in the Co ($2p_{3/2}$) signal from 780.0 eV to 778.3 eV [76]. A combination of the behaviour of the manganese as well

as the cobalt can explain the observed r.s.a.p. of 68% for the oxygen after reduction. The shape of the O (1s) signal is similar to that observed before reduction (or after Ar^+ bombardment) and after reduction in the previous study.

The catalyst surface after reduction in this study is in a similar state to the reduced catalyst in the previous study where no prior Ar^+ treatment was performed. (See Chapter 3, page 28). This allows one to assume with a good deal of confidence that Ar^+ cleaning will have little or no effect on the subsequent experiments using pure (or unpromoted) Co/MnO catalyst samples.

4.2.4. CO-hydrogenation

After 5 minutes of F-T synthesis the XPS spectrum collected in the C (1s) region indicates there is a slight increase in carbon at the surface (albeit very small). Carbon build-up at the surface increases as the catalyst is exposed to the synthesis gas for longer periods of time up to a total of 6 hours. After a total of 6 hours synthesis, the r.s.a.p. of carbon is as high as 47.7%. With longer exposures of the catalyst to the synthesis gas the r.s.a.p. of carbon is seen to decrease. (This phenomenon was also noted in the F-T study with catalyst B). The subsequent r.s.a.p.'s calculated for carbon are 32.5% and 17.7% for 12 and 24 hours F-T synthesis over the catalyst, respectively.

The carbon deposited during F-T synthesis is seen to be comprised primarily of two different types or forms. The main C (1s) signal has a BE of 285.2 eV ($\pm$ 0.3 eV) with a minor component at approximately 289.5 eV. The main signal is assigned to adsorbed alkyl species. Steinbach *et al.* [79] found evidence for $CH_{3\,(ads)}$ and $CH_{2\,(ads)}$ species at 285.8 eV and 284.9 eV over cobalt (albeit using low temperatures and CH_3Cl as a source of CH_x). Baerns *et al.* [80] found XPS evidence for carbidic and graphitic carbon formation after F-T synthesis over Fe/MnO catalysts, and the amount of carbidic carbon was shown to be linked to the activity of the catalysts. Although bulk carbides are also known to form in Fe/MnO catalysts under F-T conditions, no evidence for their formation was found in this study with the Co/MnO catalysts. Bonzel *et al.* [76] observed a carbon species with a C (1s) BE of between 284 and 286 eV during CO-hydrogenation over crystalline cobalt using a 20:1 H_2 to CO ratio at 100 kPa and 275°C . They claim difficulty in identification of this peak, but state that it may be

a hydrogenated species, possibly mixed with graphitic carbon and/or some molecular CO. No evidence of a C (1s) peak near 290 eV was found in their study.

The possibility arises that the carbon signal observed in this study with a BE of 285.2 eV could be due to an oxygenated species. The negligible oxygenate yields in the hydrocarbon product spectrum (see Table 4.2.) however, seem to limit this possibility; one would also expect an oxygenated carbon species to have a higher C (1s) BE. We therefore suggest a more likely assignment of the main type of carbon present during F-T synthesis to be due adsorbed hyrdrocarbons or "C_xH_y" species. The possibility of a short lived $CH_{3\ (ads)}$ intermediate should, however not be ruled out. This is highlighted by the high methane yield observed during the F-T reactions. (See Table 4.2). These methane yields are significantly higher than those observed with industrial iron-based catalysts studied using similar equipment [43] (also see Chapter 6 concerning H_2S poisoning over an industrial iron catalyst).

The second carbon species appears as a shoulder on the main C (1s) signal and has a C (1s) BE of between 289.0 and 290.0 eV. This binding energy is assigned to $CO_{2\ (ads)}$ species which was observed in the previous study after pure CO was passed over a reduced Co/MnO catalyst. It was shown that $CO_{2\ (ads)}$ was relatively stable at 220°C but desorbed when the temperature was increased to 260°C . The possibility of another carbon species with C (1s) BE of $\sim$ 287 eV cannot be discounted, and this could either be due to an oxygenated hydrocarbon species and/or a carbonyl species.

The results from the F-T study indicate that that the chemisorbed "C_xH_y" dissociates to form hydrocarbons in the presence of large quantities of H_2 instead of forming graphite as was the case with the pure CO experiments. (See Figure 4.7). Recently, there has been reported evidence for an oxygenated C_1 intermediate during F-T synthesis over cobalt using kinetic studies [81]. This may explain trace amounts of low molecular weight alcohols observed in the GC spectra recorded during the various F-T reactions. Furthermore, a significantly higher portion of alcohols are produced during F-T synthesis using Co/MnO catalysts compared with iron based catalysts [46]. Also there has been no evidence for carbon at a C (1s) BE of around 287 eV over industrial iron based catalysts under F-T conditions (or during pure CO treatments) studied using the same equipment as that used for this study [43]. Kinetic and reactor F-T studies on Co/MnO catalysts show that these catalysts give a slightly enhanced yield of oxygenated

products when compared to pure cobalt catalysts, and at low carbon numbers, alcohols were shown to be observed only as trace products, but at higher carbon numbers (greater than C_8) alcohols were shown to become significant products [47]. This is a reversal of the trend usually observed for alcohol yields in the F-T reaction, as methanol and ethanol are usually the most abundant alcohols [5]. Copperthwaite *et al.* furthermore claim that XPS evidence for adsorbed molecular CO over cobalt doped manganese oxide could result in the formation of alcohols via CO insertion involving the growing hydrocarbon chain, the effect of which would be more pronounced for the higher carbon numbers [82].

After one hour of F-T synthesis over the catalyst in this study, the C (1s) XPS signal is seen to shift to a higher BE of 286.4 eV and the intensity of the peak at 289.2 eV is seen to increase considerably. The peak with the C (1s) BE of 286.4 eV is assigned to oxygenated hydrocarbon species and the possibility of a $CO_{(ads)}$ species between the peaks at 286.4 and 289.2 eV, should again not be ruled out. GC data collected after one hour of F-T synthesis and prior to the sample transfer into UHV indicate that the production of low molecular weight alcohols is still negligible (see Table 4.2). The hydrocarbon product data is within reasonable agreement with that obtained for the previous and subsequent GC samplings up to the C_5 hydrocarbons. The C_6 value obtained differs considerably in that the yield is much lower. This may be explained by the presence of adsorbed CO which could, as mentioned previously, via insertion into the M-C bond lead to the formation of heavier oxygenates thereby in effect causing a considerable reduction in the amount of "heavier" hydrocarbons produced. Unfortunately, the GC equipment used was unable to detect hydrocarbons that were heavier than C_6. A point of interest is that the catalyst disc was seen to have cracked during the one hour F-T reaction, and the actual reaction temperature has been shown to be lower than the experimentally measured one[†]. The observed deviation in the C (1s) XPS spectrum after 1 hour of F-T synthesis can therefore satisfactorily be explained, since adsorbed CO and CO_2 would be expected to be more stable at lower temperatures.

During F-T treatments the cobalt r.s.a.p changes but is seen to reach a stable value after 12 hours of CO-hydrogenation (See later discussion of oxygen, manganese

[†]See Chapter 2, page 14.

and cobalt behaviour during F-T synthesis). This cobalt "steady state" may limit the amount of CO adsorption (which, coupled to the presence of H_2) could lead to hydrocarbon removal from the surface, since adsorbed alkyl groups would be hydrogenated away. This may explain the observed lowering of the r.s.a.p. of carbon which occurs when the Co/Mn surface atomic ratio stabilizes.

An increase in the amount of carbon at the surface is again associated with a decrease in the r.s.a.p. of oxygen and vice-versa. (See Figure 4.6). This correlation between the carbon and oxygen should however be seen in the context of the behaviour of the cobalt and manganese. The cobalt and manganese increase (as one would expect), is approximately proportional to that of oxygen. This fact indicates that carbon coverage occurs over the whole catalyst and not just at certain centres. Most of the carbon is unlikely to be in the form of a single chemisorbed or adsorbed species, but is more likely to be present as hydrocarbons. These hydrocarbons are shown by the GC data to have low carbon numbers (not heavier than C_6) as well as low olefin to paraffin ratios. (See Table 4.2). These factors are most probably a direct result of the high H_2 to CO ratio used in the feed gas and the high flowrates utilised. (The reasons why such conditions were employed have been discussed in Chapter 2). Comparisons of GC data obtained using the same equipment and similar reaction conditions with alkali-promoted industrial iron catalysts indicate that higher yields of methane are observed over Co/MnO catalysts. In addition, less carbon build-up is observed over Co/MnO catalysts. *Bonzel et al.* performed F-T reactions over metallic cobalt [76] and iron foils [83][84]. Employing the same conditions over both foils, these workers found that only after increasing the $CO:H_2$ ratio from 1:20 to 1.1 did the amount of carbon on cobalt approach that deposited on iron using a ratio of 1:20. In addition, hydrocarbon product distributions for the two surfaces showed the most similarity near ratios of 1:1 on cobalt and 20:1 on iron. This higher hydrogenation activity may also be used to explain the longer catalyst lifetimes observed during F-T reactor studies using Co/MnO catalysts. The absence of alkali promoters in the Co/MnO samples studied, must however be taken into account when comparing the observed hydrogenation characteristics of Co/MnO and industrial iron catalysts. This consideration will be discussed in the following chapter.

After the first 5 minutes of F-T synthesis, there is a large increase in the surface cobalt. The Co/Mn ratio increases from 0.16 after reduction to 0.65. This increase is

significantly larger than the increase observed after pure CO was passed over a reduced sample (0.12 to 0.31). Furthermore, the cobalt is seen to remain reduced during CO-hydrogenation as is witnessed by the sharp metallic Co ($2p_{3/2}$) peak at a BE of 778.2 eV. Indeed the sharpening up of the Co ($2p_{3/2}$) XPS signal coupled to the BE of 778.2 eV indicates that the cobalt becomes completely reduced during the initial stages of CO-hydrogenation.

The Co/Mn ratio fluctuates as the F-T reaction proceeds but is seen to have a stable value after 12 and 24 hours of CO-hydrogenation. This stabilised value of approximately 0.29 is close to the value of 0.30 obtained during pure CO treatments, and corresponds to a decrease in the r.s.a.p. of carbon. A possible reason for this has been cited in the discussion of the results obtained in the C (1s) region. These results lead one to the assumption that during the initial stages of F-T synthesis, the reduced cobalt is mobile.

The behaviour of the Mn ($2p_{3/2}$) signal is similar to that observed after the pure CO treatments. During F-T synthesis the Mn ($2p_{3/2}$) peak is seen to shift to a slightly higher BE of 641.0 eV and becomes narrower. There is also an indication that a shake-up satellite starts to appear, indicating the presence of MnO at the surface.

The shape of the O (1s) signal changes when the catalyst is subjected to synthesis gas, and becomes narrower. This was also observed during catalyst treatments with pure CO. Again, these changes may be explained by the observed changes in the Mn ($2p_{3/2}$) and Co ($2p_{3/2}$) peaks during CO-hydrogenation. The narrowing of the O (1s) signal may be related primarily to the narrowing of the Mn ($2p_{3/2}$) signal, and to a lesser extent to the narrower Co ($2p_{3/2}$) signal.

After a total of 30 minutes of F-T synthesis, the O (1s) signal is seen to be considerably lower compared with subsequent signals. This phenomenon should be seen in the context of the large Co/Mn ratio of 0.83 after 30 minutes F-T synthesis, compared with a rato of 0.22 after 1 hour synthesis. Obviously, the relatively high concentration of cobalt (metal) with respect to manganese (oxide) leads to a decrease in the oxygen signal.

As the F-T reaction proceeds, the Mn ($2p_{3/2}$) signals do not change significantly except for the fact that they become stronger as the Co/Mn ratio decreases. When this occurs the appearance of a shake-up satellite becomes more evident between the

Mn ($2p_{3/2}$) and Mn ($2p_{1/2}$) peaks. This fact, coupled to a Mn ($2p_{3/2}$) BE of 640.6 eV (which does not change significantly during the CO-hydrogenation experiments), may be taken as evidence that MnO is the predominant form of manganese during the F-T treatments.

As mentioned previously, virtually all the cobalt is metallic during the first 12 hours of F-T synthesis. This is in contrast with the pure CO study, where cobalt metal was re-oxidised. The high partial pressure of H_2 in the reactor during the CO-hydrogenation reactions may play a role in ensuring that oxidation of the cobalt is inhibited. After 24 hours of F-T synthesis over the sample, a shoulder at the high-BE side of the metallic Co ($2p_{3/2}$) peak is seen to appear. This indicates that some re-oxidation of the cobalt has taken place, possibly by H_2O produced during the F-T reaction.

In general, the results prior to and during the F-T treatments obtained with catalyst B resemble those obtained with catalyst A. This illustrates that reproducable results are obtainable with the instrumentation used for these studies. (See Figure 4.8).

4.2.5. Argon ion bombardment: Catalyst A

Argon ion bombardment was performed on catalyst A after it had been subjected to a total of 24 hours F-T synthesis. This treatment has the effect of removing all the surface carbon. This may be taken as evidence that no carbon build-up took place in the catalyst bulk during the CO-hydrogenation experiments. This is in contrast to findings with Fe/MnO catalysts where bulk carbide formation readily takes place during F-T synthesis [69][73]. Evidence for bulk carbide formation was however found after treatments with pure CO in the carburisation study with a Co/MnO catalyst. This finding once again illustrates the high hydrogenation activity of the Co/MnO catalyst under the conditions employed.

As was the case in the Ar^+ treatment prior to the reduction with H_2, the Co/Mn ratio decreases on bombardment. In this instance the ratio decreases from 0.27 after 24 hour F-T synthesis to approximately 0.1 after sputtering. Reasons for this decrease are the same as those given for the previous Ar^+ bombardment. The only difference being that after the second sputtering treatment, the cobalt in the bulk is slightly more oxidised than at the surface, as is witnessed by the broadened Co ($2p_{3/2}$) signal

with a significantly larger oxide component (at a BE of 7[illegible].0 eV). This is in contrast to the result obtained after the previous Ar^+ treatment where bulk cobalt was more reduced than the surface cobalt. The low r.s.a.p.'s of cobalt in both instances (6.0 and 2.2% respectively) do however, not really influence the O (1s) signal shape. Also, the cobalt after the second Ar^+ bombardment is considerably more reduced than after the first sputtering treatment. The fact that there is still a large portion of metallic cobalt present in the bulk is again indicative that reduction of the sample may start from the bulk (as mentioned in the discussion of the reduction study), and/or that the metallic cobalt is mobile in the Co/MnO system. Colley *et al.* have recently shown that a previously unreported (bulk) body centered cubic (bcc) phase of cobalt appears when F-T synthesis is performed over a similar Co/MnO catalyst [85].

The Mn ($2p_{3/2}$) spectrum is not changed by sputtering with A[illegible], thereby indicating that MnO is the predominant form of manganese in the bulk.

4.2.6. Re-reduction with H_2 : Catalyst B

Re-reduction of catalyst B after it had been subjected to a total of 24 hours F-T synthesis has the effect of removing all the carbon at the surface. This indicates that no graphitic carbon formation was likely to have taken place during F-T synthesis since graphitic carbon cannot be easily hydrogenated [86]. Graphitic carbon formation was however observed after pure CO was administered to the catalyst. (There was also no evidence for carbidic carbon formation, as witnessed by the high BE of the C (1s) signal during CO-hydrogenation). A GC sample was taken 10 minutes after the start of the 12 hour re-reduction. This indicated that virtually only methane was desorbing from the catalyst surface. (Compare Figures 4.9 and 4.10). The above findings all indicate that the assignments of the C (1s) BE's during the various treatments are realistic.

Re-reduction of catalyst B has little effect on the XPS signal shapes of the O (1s), Mn ($2p_{3/2}$) and Co ($2p_{3/2}$) spectra. The Co/Mn ratio was however again shown to decrease after this H_2 treatment (0.38 to 0.12), and possible reasons for this have already been discussed.

4.3. Conclusions

Various carbon species are deposited over the catalyst during CO-hydrogenation. One being assigned to light hydrocarbons, possibly "CH_x" and/or "C_xH_y" adsorbed on cobalt, and the other being chemisorbed CO_2. The C_xH_y species desorb to form light hydrocarbons in the presence of H_2 instead of graphite, as is the case when pure CO gas is used. There is also some evidence for $CO_{(ads)}$, and this species may be inserted into the growing hydrocarbon chains, thereby explaining higher alcohol yields observed when using these catalysts (compared to iron F-T catalysts), and the traces of low molecular weight alcohols observed in this study.

The build-up of carbonaceous material is less marked during CO-hydrogenation over Co/MnO catalysts compared to Fe/MnO and industrial iron based catalysts treated under similar conditions. There is also no build-up of carbonaceous material in the catalyst bulk, and this further highlights the higher hydrogenation activity observed with Co/MnO.

During CO-hydrogenation, the cobalt remains reduced, whilst MnO is the predominant form of manganese at the surface. The cobalt concentration at the surface fluctuates before stabilising during CO-hydrogenation, and this behaviour is linked to the amount of surface carbon present.

4.4. Data collected for the CO-hydrogenation study with pure cobalt-manganese oxide catalysts

See following pages.

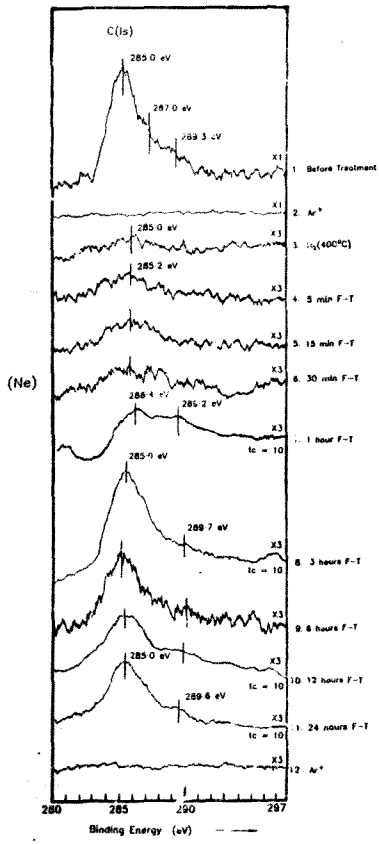

Figure 4.1. XPS spectra recorded in the C (1s) region between various treatements, for the CO-hydrogenation study with Co/MnO.

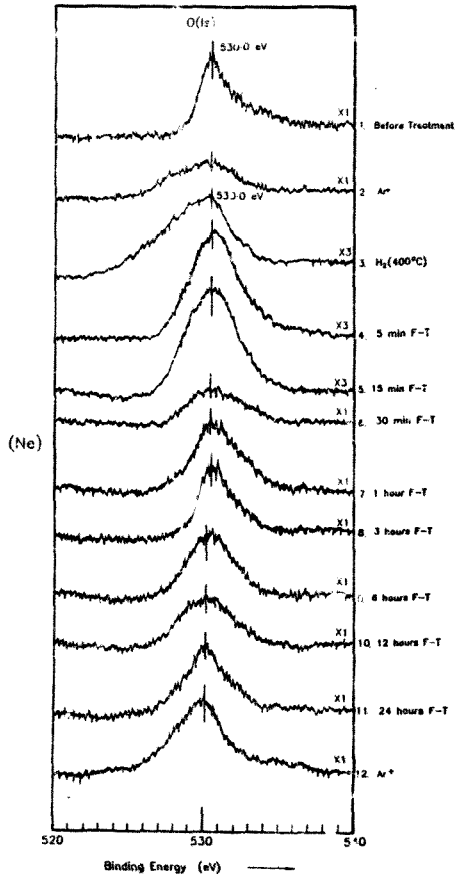

Figure 4.2. XPS spectra recorded in the O (1s) region between various treatments, for the CO-hydrogenation study with Co/MnO.

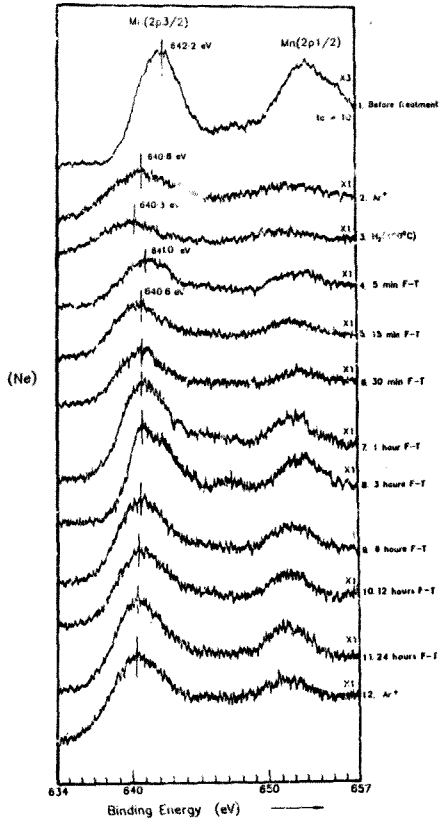

Figure 4.3. XPS spectra recorded in the Mn ($2p_{3/2}$) region between various treatments, for the CO-hydrogenation study with Co/MnO.

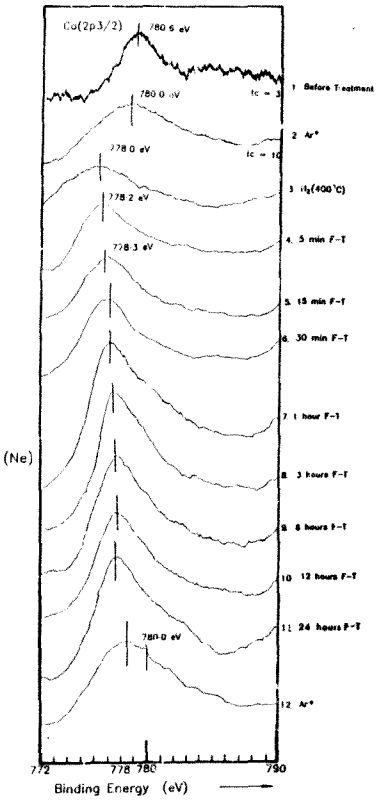

Figure 4.4. XPS spectra recorded in the Co ($2p_{3/2}$) region between various treatments, for the CO-hydrogenation study with Co/MnO.

	R.S.A.P.'s OF ELEMENTS BETWEEN TREATMENTS			
TREATMENT	C	O	Mn	Co
1	32.9	50.6	9.7	6.8
2	0.0	74.0	20.0	6.0
3	0.0	68.5	26.8	4.7
4	TR	55.3	27.0	17.7
5	22.1	51.5	15.3	11.1
6	26.0	55.0	10.4	8.6
7	33.4	56.7	8.1	1.8
8	40.5	49.3	7.2	3.0
9	47.7	41.3	6.7	4.3
10	32.1	48.3	14.9	4.3
11	17.7	66.6	12.3	3.3
12	0.0	76.3	21.5	2.2

Table 4.1. **Relative surface atomic percentages of elements between the various treatments, for the CO-hydrogenation study with Co/MnO.**

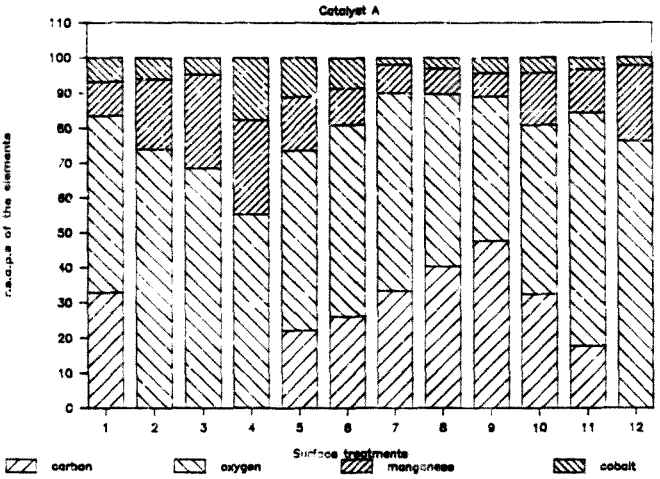

Figure 4.5. Graphic illustration of relative surface atomic percentages (r.s.a.p.'s) of elements between treatments, for the CO-hydrogenation study with Co/MnO.

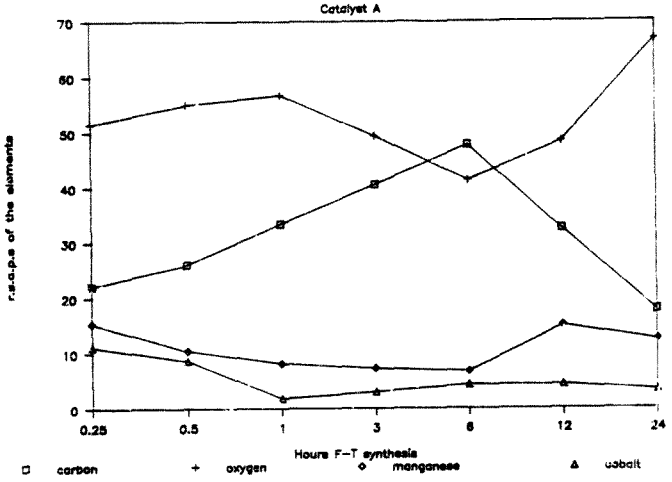

Figure 4.6. Plot of r.s.a.p. trends after the various treatments, for the CO-hydrogenation study with Co/MnO.

	MASS/MASS % HYDROCARBON SELECTIVITY									
TREATMENT	C1	C2=	C2	C3=	C3	C4	C5	C6	MeOH	EtOH
15 min. F-T.	64.0	0.2	14.5	0.3	8.6	5.7	2.5	3.5	TR	TR
1 hour F-T.	59.6	0.2	13.9	13.7	6.3	7.2	1.7	0.1	"	"
3 hours F-T.	63.4	0.1	11.4	0.5	6.6	6.3	3.9	5.7	"	"
6 hours F-T.	71.6	0.1	13.7	0.2	4.2	3.6	1.5	4.6	"	"
12 hours F-T.	66.0	0.1	11.6	0.1	7.3	4.5	1.7	4.9	"	"
24 hours F-T.	77.6	0.1	11.6	0.1	3.4	1.9	0.9	4.5	0.0	0.0
12 hours H_2 (Catalyst B)	98.8	0.1	0.7	TR	TR	TR	TR	TR	0.0	0.0

Table 4.2. Mass/Mass % of hydcarbon components detected during various CO-hydrogenation treatments over Co/MnO.

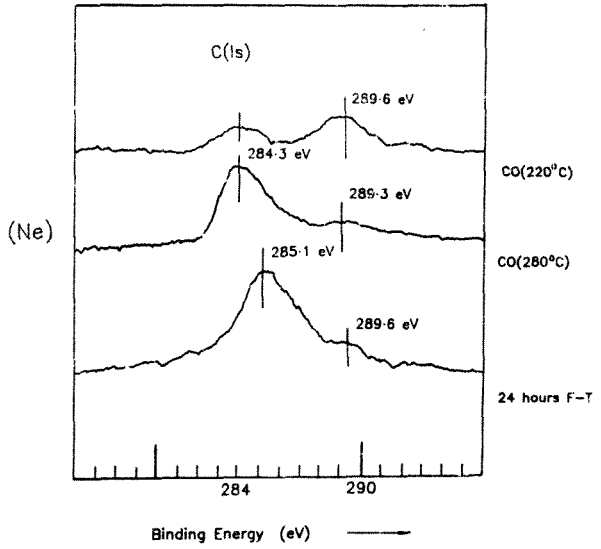

Figure 4.7. Comparison of C (1s) spectra recorded after carburisation and CO-hydrogenation treatments.

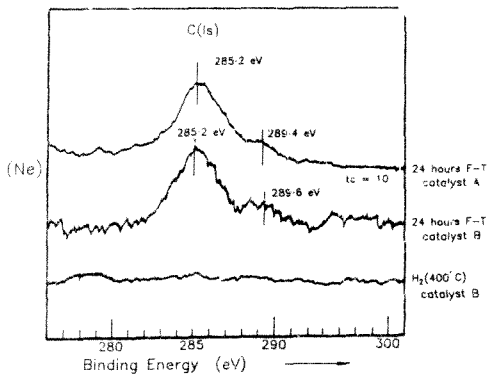

Figure 4.8. Comparison of C (1s) spectra recorded after 24 hours F-T synthesis over catalysts A and B, as well as the C (1s) spectrum recorded after the final H_2 treatment over catalyst B.

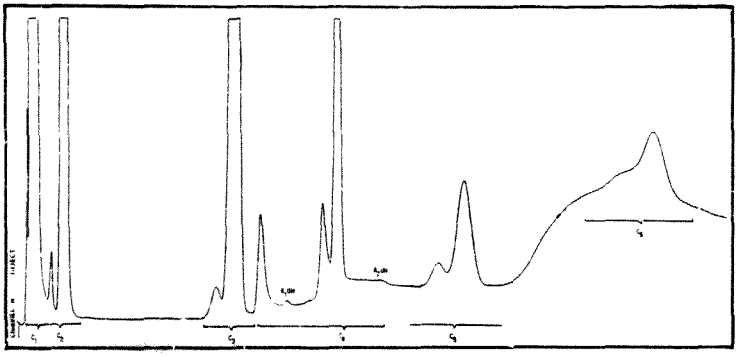

Figure 4.9. GC trace recorded at 24 hours F-T synthesis over catalyst B.

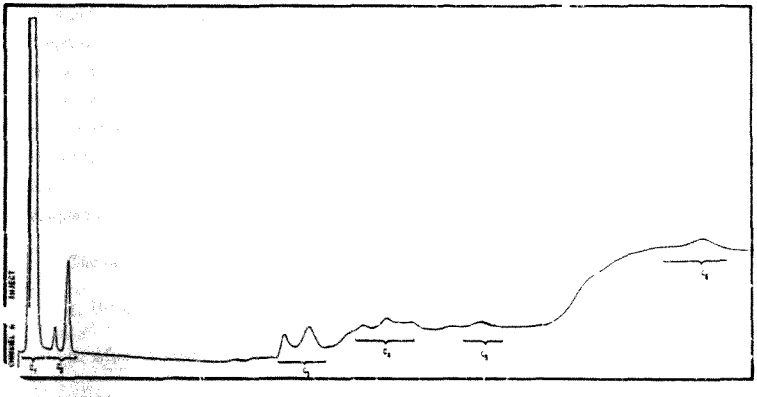

Figure 4.10. GC trace recorded at 10 minutes re-reduction over catalyst B, after the catalyst had undergone a total of 24 hours F-T synthesis.

Chapter 5. CO-hydrogenation over a potassium-promoted cobalt-manganese oxide catalyst

5.1 Experimental route

Conditions similar to those employed with the unpromoted Co/MnO catalyst were used. A 0.25% potassium-promoted Co/MnO catalyst with a Co/(Co + Mn) bulk ratio of 0.47 was studied both under reducing as well as CO-hydrogenation conditions. Preparation of the Co/MnO catalyst has been reported elsewhere [47][48]. Promotion of the catalyst was achieved using the incipient wetness technique before subsequently calcining the catalyst in air. Colley *et al.* [87] have performed bulk (using XRD) and reactor studies on potassium-promoted Co/MnO catalysts, the results of which are compared with those obtained in this study. These reactor studies have shown that K_2CO_3 loadings of around 0.25% gives rise to the highest C_2 and C_3 olefin selectivities coupled to low methane production.

The catalyst was analysed by XPS in the following sequence:

1. Before treatment.
2. After 12 hours H_2 (400°C).
3. After 15 minutes F-T synthesis.
4. After 1 hour F-T synthesis.
5. After 3 hours F-T synthesis.
6. After 6 hours F-T synthesis.
7. After 12 hours F-T synthesis.
8. After 12 hours H_2 (400°C).
9. After Ar^+ bombardment (5 kV beam energy for 5 minutes).

5.2. Results and discussion

The text refers to the C (1s), K (2p), O (1s), Mn ($2p_{3/2}$) and Co ($2p_{3/2}$) XPS spectra recorded between the various treatments, and compares the results with those discussed in the previous two chapters. The spectra, as well as various tables and graphs, are shown at the end of this chapter. The r.s.a.p.'s of the elements detected at the surface between the various treatments are quoted in Table 5.1.

5.2.1. Untreated catalyst

Before treatment, the carbon C(1s) peak has a pronounced shoulder with a BE of 289.6 eV. As mentioned for the previous studies, this again is assigned to a $CO_{2\ (ads)}$ species, but in this case is also due to surface carbonate from K_2CO_3. Thermogravimetric analysis during heating of samples of pure K_2CO_3 in both ambient (oxidising) and H_2 atmospheres have shown that K_2CO_3 is thermally stable up to 850°C [88].

The main C (1s) signal has a BE of 286.0 eV and is assigned to oxygenated hydrocarbon contamination.

The r.s.a.p. of potassium of 6%, compared with a bulk concentration of 0.25%, is indicative that calcining the catalyst facilitates segregation of potassium to the surface. The K (2p) signal at a BE of 293.6 eV is broad and does not have a clear doublet structure, as does K_2O and KOH [51][85][90] (observed on iron catalysts with potassium promotion) or pure K as studied on cobalt by Bonzel *et al.* [76]. The peak shape may be attributed to the fact that a relatively low concentration of potassium was added to the catalyst (0.25%), and not that the potassium is added in the form of K_2CO_3. C (1s) and K (2p) spectra of pure, untreated K_2CO_3 show that the K (2p) peak is in the form of a 2:1 doublet and there is a C (1s) signal at 290.0 eV presumably from CO_3^{2-}. (See Figure 5.2)

There is some difficulty in the identification of the broad signal at the high BE side of the K ($2p_{3/2}$) and K ($2p_{1/2}$) peaks. After considering all the various options (XPS and AES transitions of all elements expected to be in the sample, as well as possible impurities and incorrect sample position), we believe it could either be a Ta (MNN) or an Au (MNN) Auger transition arising from the sample holder. Moreover, this signal is

not present in pure K_2CO_3 which was measured using a different sample holder. (See Figure 5.2).

Prior to treatments, the Co/Mn surface ratio is 0.45. Taking the r.s.a.p. of 18.1% for carbon into account, this value is in line with Co/Mn ratios before treatments in the previous two studies namely, reduction, carburisation and CO-hydrogenation of unpromoted Co/MnO. The Mn ($2p_{3/2}$) signal has a maximum at 640.0 eV, and there is no clear evidence of a shake-up satellite. This is in contrast with the unpromoted Co/MnO, where the surface manganese was shown to be more oxidised prior to treatments with the Mn ($2p_{3/2}$) peak being at 642.0 eV. (Presence of shake-up satellites is shown more clearly for the Mn ($2p_{3/2}$) and Mn ($2p_{1/2}$) spectra recorded at higher sensitivities in Figure 5.6). The fact that this peak is slightly broader than the subsequent Mn ($2p_{3/2}$) signals may obscure a shake-up satellite. The observed shape of the peak may be explained by the presence of Mn_3O_4 coupled to the presence of alkali promoter at the surface. The surface manganese of the calcined catalyst is not as oxidised as was the case with pure Co/MnO samples, indicating that CO_3^{2-} ions may be in lattice sites previously occupied by excess O^{2-} ions, with K^+ being in the cation vacancies.

The Co ($2p_{3/2}$) signal is clearly due to Co^{2+} as indicated by the BE of the peak at 780.3 eV and the shake-up satellite associated with a high-spin (d^7) configuration.

The fact that the cobalt peak BE is consistent with Co ($2p_{3/2}$) signal BE's for calcined samples before treatments in the previous studies, coupled to the fact that the surface manganese is less oxidised, may be indicative that the alkali promoter is localised and associated with the manganese oxide lattice.

The O (1s) signal is asymmetric in that it is broader on the high BE side of the peak. The shape of the signal is similar to the O (1s) signal observed for the unpromoted catalyst F-T study prior to treatments. The asymmetric oxygen signal may be due to various oxides of manganese and cobalt, but is most probably due to oxygenated carbon, specifically carbonate from K_2CO_3. The r.s.a.p.'s of oxygen and potassium are 56.8 and 6% respectively. If all the potassium is in the form of K_2CO_3, this implies that 9/56 x 100% (or approximately 16%) of the O (1s) signal is caused by the high BE shoulder. The fitted data shows that a larger portion than 16% constitutes the high BE shoulder

on the O (1s) signal. and this is probably due to oxygen from $CO_{2\,(ads)}$ species which have also been observed over untreated Co/MnO without potassium promotion.

5.2.2. Reduction with H_2

Reduction with H_2 for 12 hours has the effect of removing all the carbon with a BE of 286.0 eV, but there is still carbon present with a BE of 290.6 eV. This is in contrast to reductions performed in the previous studies with unpromoted Co/MnO where all the carbon is seen to be removed by reduction at 400°C . Reduction and CO-hydrogenation of industrial iron catalysts with K_2O loadings of approximately 0.2, 0.4 and 0.6%, have been studied [43]. (Also see Chapter 6). These studies show that reduction of untreated samples gives rise to graphitic carbon formation (from the original hydrocarbon surface contamination), and this process is seen to be more easily facilitated on the iron catalysts with higher K_2O loadings.

The fact that a C (1s) BE of around 290 eV has been associated with an adsorbed CO_2 species (which are known to desorb with increased temperature), may be taken as evidence that the peak at 290.6 eV is now associated with the carbonate of the K_2CO_3 promoter. This also gives credibility to the argument that adsorbed CO_2 on Co/MnO has a C (1s) BE around 290 eV. The r.s.a.p.'s of carbon (5.1%) and potassium (10.1%) indicate that most, if not all of the potassium is in the form of K_2CO_3 after reduction. This finding is in contrast to reported evidence by Bonzel *et al.* who suggest the presence of KOH after the reduction of KNO_3, K_2CO_3 and KOH promoted iron and platinum surfaces [91]. These workers however, employed different conditions in that samples were annealed in UHV using temperatures of up to 690 K. This was performed prior to reduction with H_2 at 570 K in a reactor interfaced to the UHV chamber. After heating of their samples in UHV, the KNO_3 and K_2CO_3 were shown to be in various states of decomposition.

The r.s.a.p. of potassium after reduction increases from 6.1% to 10.1% and is associated with a change in shape of the K (2p) XPS signal which is seen to more closely approach that of a doublet (albeit not a clear 2:1 doublet associated with K_2O and KOH, observed over an industrial catalyst (see sulphur poisoning study) and potassium metal over cobalt [76]). The high r.s.a.p. of potassium is indicative that the promotor

segregates to the surface. This is consistent with other studies that have observed surface mobility of potassium promoters [43][80].

Treatment with H_2 has the effect of lowering the Co/MnO ratio from 0.45 to 0.25. The Co/Mn ratio after reduction is however considerably higher than the ratios after reduction over *unpromoted* Co/MnO, which was shown to give a ratio in the region of 0.15. This difference is obviously due to potassium promotion of the Co/MnO, but can be explained on examination of the cobalt and manganese XPS spectra, more specifically, by differences between the cobalt and manganese spectra of the promoted catalyst after reduction with respect to unpromoted catalysts after the same treatment.

After reduction the Mn ($2p_{3/2}$) signal becomes narrower and a shake-up satellite becomes more evident. (This is shown more clearly with the manganese spectra recorded at higher sensitivities in Figure 5.6). The H_2 treatment therefore gives rise to MnO. This behaviour for manganese was observed with H_2 treatments over unpromoted Co/MnO, but the concentration of MnO in the potassium promoted sample is higher, as is witnessed by the clearer shake-up satellite.

The Co ($2p_{3/2}$) signal of the K-promoted sample after treatment with H_2 differs with those observed with pure Co/MnO after the same treatment. In the studies using *unpromoted* Co/MnO catalysts, reduction of the cobalt at the surface was more easily facilitated, and shown to be complete. In this study, reduction of the surface cobalt is *incomplete*, as shown by the broader Co ($2p_{3/2}$) signal with the metallic and oxide components. The presence of Co^{2+} is confirmed by the shake-up satellite, which is still present (albeit supressed). The preceding studies have led to the assumption that metallic cobalt may be mobile, and that reduction may start in the bulk. These assumptions, as well as the incompletely reduced cobalt at the surface may explain the higher than expected Co/Mn ratio after reduction. Obviously potassium inhibits reduction of the catalyst surface and this is clearly shown by the behaviour of the cobalt. The presence of K_2CO_3 would lower the number of cation vacancies in the MnO lattice, resulting in the metallic cobalt having a lower diffusion capability.

If one considers the Co ($2p_{3/2}$) signal after Ar^+ bombardment at the end of the study, it is clear that the cobalt in the catalyst bulk is considerably more reduced than at the surface, as is shown by the sharp peak at a BE of 778.3 eV and the disappearance of the shake-up satellite associated with Co^{2+}. The fact that there is no potassium

after the final Ar^+ treatment gives credibility to the above arguments concerning the mechanism of reduction coupled to the behaviour of the cobalt and the effect alkali may have on these.

The r.s.a.p.'s calculated for carbon and potassium after the H_2 treatment indicate that all the surface carbon (5.1%) originates from K_2CO_3. The K:C:O ratio for potassium carbonate is 2:1:3, this implies that O^{2-} from the carbonate constitutes approximately 15% of the atoms at the surface, or 15/60.9 x 100% of the area of the O (1s) signal. Indeed, a high BE shoulder on the O (1s) peak constituting approximately 25% of the O (1s) peak area is observed after the H_2 treatment.

The shape of the O (1s) signal after reduction also differs from that observed after the same treatment over unpromoted Co/MnO in that there is no broad shoulder at the *low* BE side of the main peak at 530.0 eV. The reasons for this are not clear, but may lie in the difference between the Mn ($2p_{3/2}$) spectra of the unpromoted and promoted samples after reduction. The most obvious difference being that the Mn ($2p_{3/2}$) signal of the promoted catalyst is slightly narrower and and the shake-up satellite is more obvious after treatment with H_2. The cobalt spectrum in the promoted sample is also different, in that the cobalt is not completely reduced. Furthermore, the cobalt remains incompletely reduced during subsequent CO-hydrogenation treatments, and the O (1s) spectra more closely approximate those of an unpromoted sample during these treatments. This leads to the deduction that the differences in the O (1s) spectra after reduction of unpromoted and promoted Co/MnO are in fact, largely due to differences in the Mn (2p) spectra.

5.2.3. CO-hydrogenation

After 15 minutes F-T synthesis over the potassium promoted Co/MnO catalyst, carbon with a BE a C (1s) of 285.1 eV is seen to appear and this is once again assigned to hydrogenated carbon species. The peak with a BE of 289.5 eV is seen to increase relative to the K (2p) signal which retains it's doublet shape. This high BE C (1s) signal can therefore be attributed to adsorbed CO_2 and carbonate from K_2CO_3. As is the case with unpromoted Co/MnO, there is no evidence for graphitic or carbidic carbon after exposure to synthesis gas.

The Mn ($2p_{3/2}$) signal remains virtually unchanged during the F-T treatments, indicating that the manganese at the surface remains in the form of MnO.

The Co ($2p_{3/2}$) signal indicates that the oxide component at a BE of 780.5 eV increases, and this is highlighted by the appearance of a more prominent shake-up satellite. The Co/Mn ratio increases from 0.25 to 0.36 which is approximately the same value as was observed after pure CO treatments of unpromoted Co/MnO, which had the effect of oxidizing the cobalt to CoO.

The O (1s) spectrum is seen to remain virtually unchanged during F-T synthesis, and the continued presence of a high BE shoulder, can be attributed to a mixture of oxygenated carbon species, namely $CO_{2\,(ads)}$, CO_3^{2-} (from K_2CO_3) and to a lesser extent $CO_{(ads)}$. It is interesting to note that in the previous CO/H_2 study with unpromoted Co/MnO, that a high BE shoulder appeared on the O (1s) signal when oxygenated carbon species where observed at the surface. (See Figures 4.1 and 4.2 with respect to treatment 8).

The GC trace recorded at 15 minutes F-T synthesis indicates that the potassium has a profound effect on the hydrocarbon distribution when compared to a GC spectrum taken at the same time (with the same reaction conditions employed) but using unpromoted Co/MnO. Potassium has the effect of lowering methane production, increasing the the olefin to parrafin ratio and increasing the average hydrocarbon chain-length. (See Table 5.2 of M/M % hydrocarbons after the various treatments). These findings correspond well to bulk reactor studies performed with these catalysts [87], which show that potassium promotion increases the low molecular weight alkene/alkane ratios (C_2 and C_3), and decreases methane selectivity. (See Table 5.3).

After 1 hour F-T synthesis the C (1s) peak at 285.1 eV is seen to have increased whilst that from the adsorbed CO_2 and/or carbonate species is supressed. The K (2p) signals are also lower. The increased intensity of the C (1s) signal at 285.1 eV is associated with a decrease in methane production and an increase in the average hydrocarbon chain-length. The Co/Mn ratio increases marginally from 0.34 to 0.38 and the CoO component in the Co ($2p_{3/2}$) signal is slightly increased, whilst the Mn ($2p_{3/2}$) and O (1s) signals are unchanged.

After 3 hours F-T synthesis the intensity of the C (1s) peak at a BE of 285.1 eV decreases considerably, whilst the potassium and oxygenated carbon signals are enhanced. Overall, there is a large decrease in the amount of carbon at the surface (the r.s.a.p. is lowered from 12.7 to 6.2%). These changes are reinforced by the increases in the r.s.a.p.'s of all the other elements. The GC spectrum recorded at 3 hours synthesis indicates a reversal in the hydrogenation activity of the catalyst when the surface is in this condition. (See Table 5.2). Methane production increases to approximately 84% and the average hydrocarbon chain-length decreases. Again, as was the case in the F-T study with an unpromoted catalyst, a convenient explanation for the deviation in hydrogenation activity is forthcoming when one considers the experimental conditions of the reaction. The actual temperature of the catalyst was shown to be lower than the measured one. (See Chapter 2, page 14). This explains the stabilised $CO_{2\ (ads)}$ peak, and the possible decreased propensity for CO dissociation would explain the low intensity hydrocarbon C (1s) peak at 285.1 eV, as well as the significant increase in methane production, coupled to the smaller percentage of C_3 to C_6 hydrocarbon formation. Furthermore this "error" highlights the temperature dependance of the selectivity for this F-T reaction which in turn could have important consequences on the catalyst lifetime. The fact that on removal of of a large portion of the carbon with a C (1s) BE at 285.1 eV exposes the potassium signal (and results in an increase in the r.s.a.p.'s of the other elements) is again indicative that this carbon signal is due to hydrogenated carbon or alkyl species.

F-T reactions over the catalyst were carried out up to a total of 12 hours. After 6 and 12 hours F-T synthesis, the hydrogenated carbon species is seen to increase and the r.s.a.p.'s of carbon are 28.6 and 32.3% respectively. There is also evidence suggesting a carbon species with a C (1s) BE of 288.0 eV, and this may be due to an oxygenated hydrocarbon or $CO_{(ads)}$ species. This species is more obvious over Co/MnO with potassium promotion compared to pure Co/MnO after 6 and 12 hours F-T synthesis. (See Figure 5.3). This may explain the higher oxygenated hydrocarbon production observed during CO-hydrogenation over potassium promoted Co/MnO with bulk reactor studies. (See Table 5.3). These reactor studies show that potassium promotion increases the production of heavier alcohols. This may be linked to the evidence for increased $CO_{(ads)}$ species on the catalyst, which could via CO insertion into

the growing hydrocarbon chains, result in alcohol formation. As mentioned previously, this effect would be more pronounced for higher carbon numbers [82].

The results from the present study show that an increase in the C (1s) signal with a BE of 285.1 eV is associated with an increase in the metallic component of the Co ($2p_{3/2}$) XPS signal, and these findings are consistent with those in the previous F-T study using unpromoted Co/MnO.

CO adsorption studies over potassium (metal) promoted, and unpromoted cobalt foil undertaken by Bonzel *et al.* [76] claim evidence that alkali has the effect of decreasing the C (1s) BE of molecular CO due to enhanced electron density on the CO molecule. These workers showed that potassium enhances the the amount of CO adsorbed and thermally stabilises the adsorbed molecule, resulting in increased carbon deposition due to the enhancement of the CO adsorption step. Indeed, numerous studies have shown that potassium facilitates the decomposition of CO [92-95]. Bonzel *et al.* also showed that the presence of potassium results in carbidic (and not graphitic) carbon formation, and that the reactivity of this species is lowered by potassium, thereby helping to explain the lower methanation rates observed with potassium- promoted F-T catalysts [76].

The amount of carbon deposited during F-T synthesis on the catalyst in the present study does not differ markedly with respect to unpromoted Co/MnO, although one would expect to see enhanced carbon build-up due to potassium-promotion. One reason why this is not observed may be due to the chosen operating conditions, in that the F-T reactions are seen to be performed in a critical temperature region. (See preceding discussion on temperature monitoring). A more likely reason however, is that the carbon (or more specifically, hydrocarbon) observed at the surface has been shown to be associated with metallic cobalt, and K_2CO_3 promotion of the Co/MnO catalyst inhibits reduction of the surface cobalt. A fact that can be used to further substantiate this argument are reports of potassium delaying graphitization and carbon build-up on iron *oxide* surfaces [96][97].

5.2.4. Re-reduction with H_2

The catalyst was re-reduced after 12 hours F-T synthesis, resulting in significant changes in the C (1s), K (2p) and Co (2p) XPS spectra.

Re-reduction has the effect of removing most, but not all the surface carbon. There is still a C (1s) peak at a BE of 285.1 eV associated with surface hydrocarbon species. A slightly lower BE (around 284.4 eV) for this peak would be indicative of graphitic carbon which is inert to hydrogenation. Re-reduction of an unpromoted Co/MnO catalyst (in the preceding study) which had been subjected to 24 hours of F-T synthesis was shown to remove all the surface carbon. The fact that not all the carbon at the surface is removed by reduction confirms that most of the remaining carbon may have graphitic characteristics. After the re-reduction there is some evidence for the presence of carbonate as indicated by the slight "hump" between the C (1s) peak at 285.1 eV and the K (2p) signal. Reduction of the untreated catalyst showed a C (1s) signal at 289.6 eV which was assumed to be from CO_3^{2-} in K_2CO_3. There is also no reason to suspect that the signal (which is not very clear) around 290 eV (after re-reduction) is not due to K_2CO_3. (Also see Figure 5.2. showing the C (1s) and K (2p) spectra of pure K_2CO_3). Removal of a large portion of the carbon exposes the potassium as shown by the r.s.a.p. increase from 4.5 to 8.9% for potassium.

Re-reduction of the catalyst has no effect on the Co/Mn ratio which is seen to remain unchanged at 0.32. The surface cobalt is largely re-oxidised as shown by the sharp Co ($2p_{3/2}$) signal at 779.7 eV which has a clear shake-up satellite indicating the presence of Co^{2+}. The behaviour of the cobalt after this treatment is in contrast with that observed for unpromoted catalyst. On re-reduction of the unpromoted catalyst the Co/Mn ratio decreased to 0.12, and only metallic cobalt was observed at the surface. The influence that the alkali promoter has on facilitating these differences has been discussed with the results for the reduction of the untreated sample in this study.

Re-reduction has no visible/marked effect on the O (1s) and Mn (2p) XPS signals.

5.2.5 Argon ion bombardment

Finally, a mild argon ion bombardment treatment was performed to ascertain the possible differences between the surface and the bulk catalyst. This treatment is shown to result in the removal of all the potassium, as is witnessed by the disappearance of the K (2p) signal. Removal of the potassium is therefore indicative that it segregates to the surface or near surface both before and during the various treatments. This corresponds

with XRD findings which show that potassium promotion at the levels investigated here does not in any way effect the bulk structure of Co/MnO catalysts [87].

A trace amount of carbon at C (1s) BE's of 284.4 eV and 283.3 eV may be taken as weak evidence for graphitic and carbidic carbon, respectively, with a possibility of some hydrogenated carbon due to the broad C (1s) signal(s) observed. The promoter is expected to have a considerable influence on the catalyst surface area and it is possible that this increase may be associated with increased porosity which would facilitate some carbon build-up in the catalyst bulk. The presence of carbon after treatment with H_2 may also be linked to the lower hydrogenation activity observed with promoted Co/MnO.

Apart from increases in the r.s.a.p.'s, of oxygen and manganese, only the O (1s) signal changes slightly after Ar^+ bombardment in that it is seen to become slightly narrower. This is presumably due to the removal of oxygen originating from K_2CO_3.

Furthermore, Ar^+ bombardment indicates that that the sub-surface cobalt is metallic as witnessed by the sharp Co ($2p_{3/2}$) peak at 778.3 eV and the disappearance of the shake-up satellite associated with Co^{2+} or CoO. This reduced cobalt is associated with removal of the potassium and gives credibility to the assumptions that reduction is initiated in the catalyst bulk and that the metallic cobalt is mobile. This is coupled to the idea that potassium inhibits reduction of cobalt at the surface.

5.3. Conclusions

Surface segregation of the potassium carbonate takes place before and during the various treatments.

Before treatment, the manganese at the surface is less oxidised compared with unpromoted Co/MnO. This indicates that CO_3^{2-} may be present in lattice sites previously occupied by excess O^{2-} ions, along with K^+ in the cation vacancies. This limits the diffusion of metallic cobalt (previously claimed to have become reduced in the bulk) through the MnO lattice, and explains why cobalt in the catalyst bulk is more reduced than at the surface.

After H_2 treatment, the carbonate component in K_2CO_3 remains intact. The presence of alkali promoter inhibits efficient reduction of the surface cobalt. This is shown to effect the amount of carbon deposited over the catalyst during the subsequent CO/H_2 treatments, since previous work with unpromoted Co/MnO has shown that the amount of metallic cobalt influences the surface carbon concentration.

The potassium promoter lowers the hydrogenation activity of the catalyst during the CO/H_2 treatments when operating at 190°C . Evidence for small amounts of adsorbed CO can be used to explain the increased tendency for alcohol production over K_2CO_3 promoted Co/MnO.

5.4. Data collected for the CO-hydrogenation study with potassium promoted cobalt-manganese oxide catalysts

See following pages

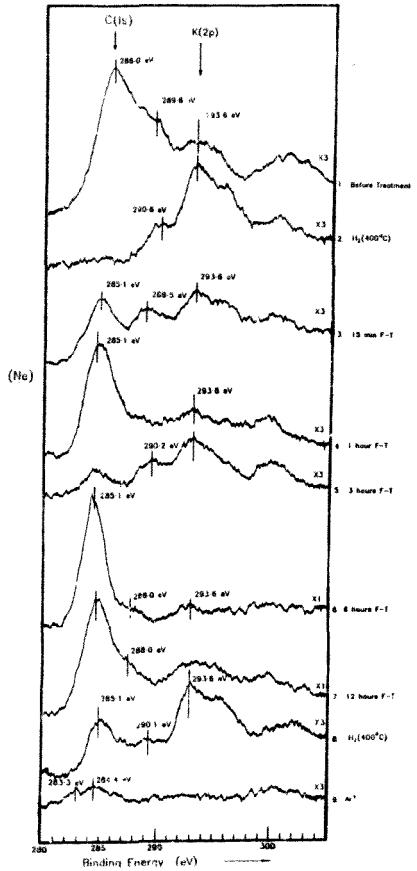

Figure 5.1. XPS spectra recorded in the C (1s) and K (2p) regions between various treatments, for the CO-hydrogenation study with K-promoted Co/MnO.

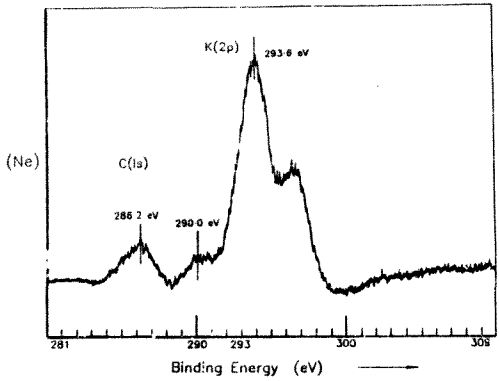

Figure 5.2. XPS spectrum recorded in the C (1s) and K (2p) regions of pure, untreated K_2CO_3.

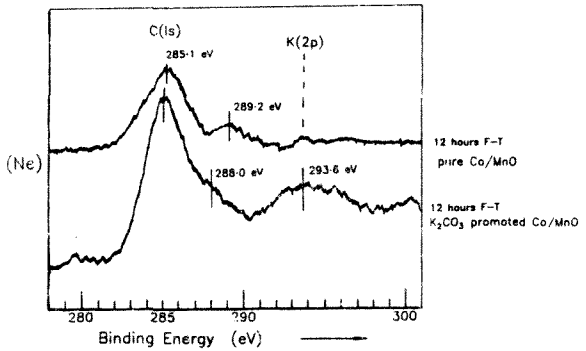

Figure 5.3. Comparison of XPS spectra recorded in the C (1s) and K (2p) regions after 12 hours CO-hydrogenation over pure and K-promoted Co/MnO.

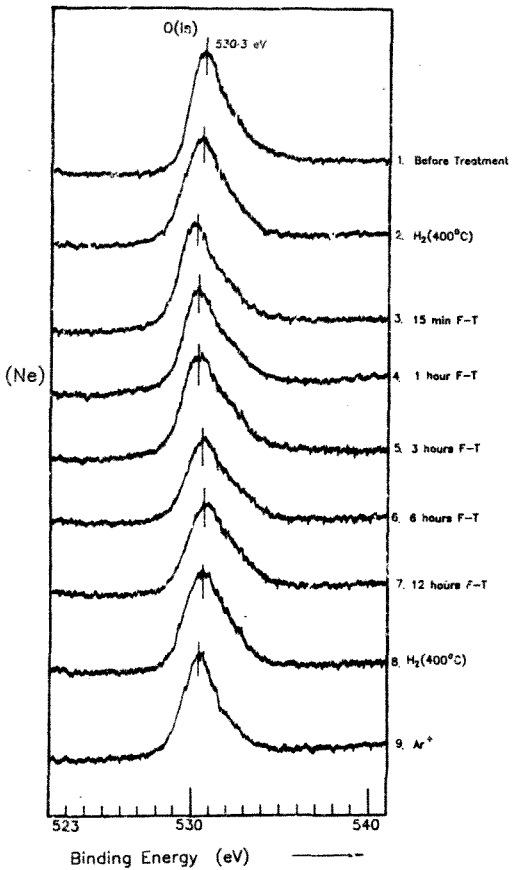

Figure 5.4. XPS spectra recorded in the O (1s) region between various treatments, for the CO-hydrogenation study with K-promoted Co/MnO.

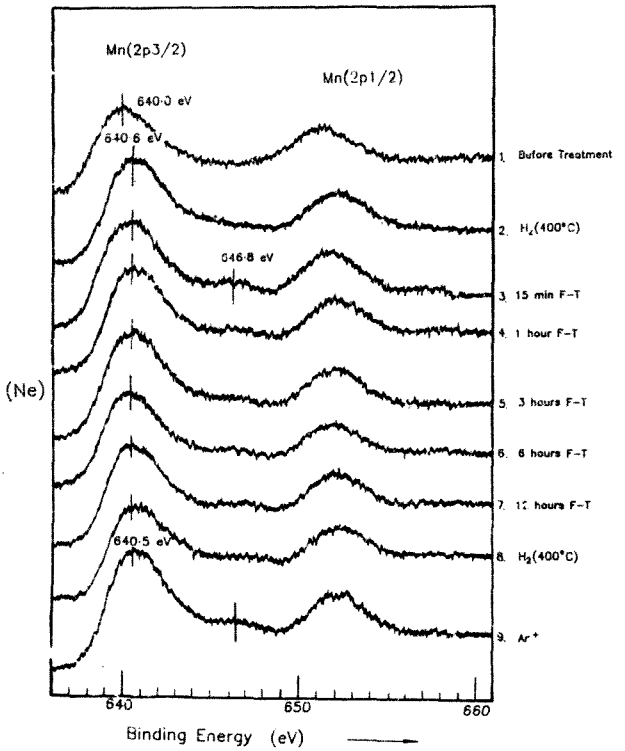

Figure 5.5. XPS spectra recorded in the Mn $(2p_{3/2})$ and Mn $(2p_{1/2})$ region between various treatments, for the CO-hydrogenation study with K-promoted Co/MnO.

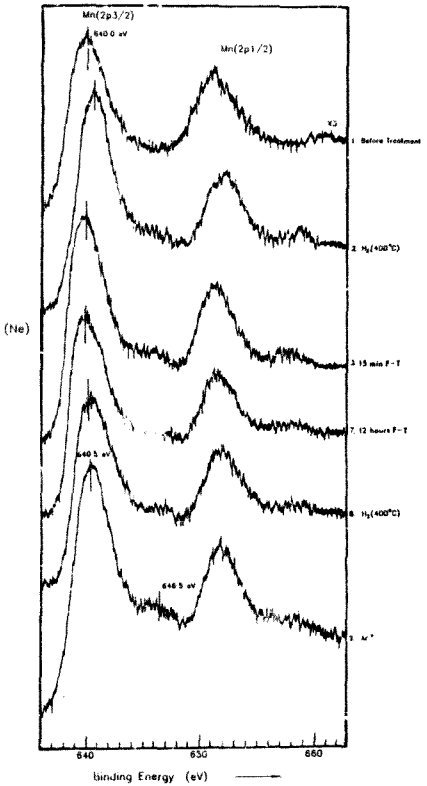

Figure 5.6. XPS spectra recorded in the Mn ($2p_{3/2}$) and Mn ($2p_{1/2}$) region at higher sensitivity, for the CO-hydrogenation study with K-promoted Co/MnO.

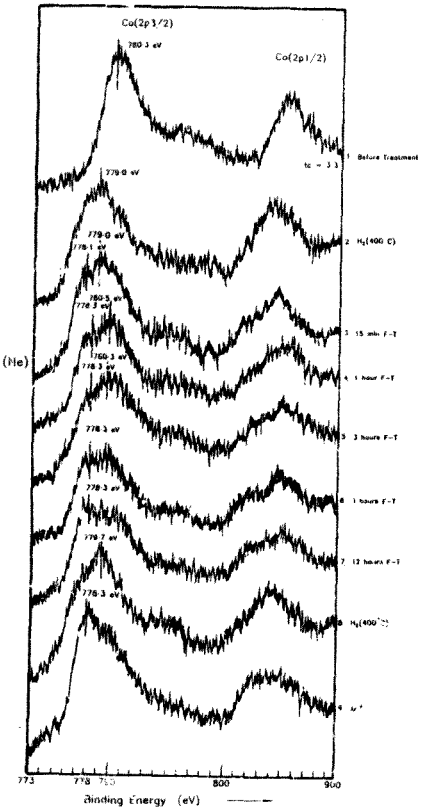

Figure 5.7. XPS spectra recorded in the Co $(2p_{3/2})$ and Co $(2p_{1/2})$ region between various treatments, for the CO-hydrogenation study with K-promoted Co/MnO.

	R.S.A.P.'s OF ELEMENTS BETWEEN TREATMENTS				
TREATMENT	C	O	Mn	Co	K
1	16.1	56.3	13.2	5.9	8.0
2	5.1	60.1	19.6	4.4	10.0
3	7.9	60.4	18.9	6.6	6.2
4	12.7	59.3	19.1	7.2	1.7
5	8.2	63.1	20.9	7.7	2.1
6	28.6	49.1	16.4	5 9	TR
7	32.3	42.8	15.8	5.0	4.5
8	7.9	57.4	19.5	6.3	8 9
9	TR	63.6	27 2	9.2	0.0

Table 5.1. Relative surface atomic percentages of elements between various treatments, for the CO-hydrogenation study with K-promoted Co/MnO.

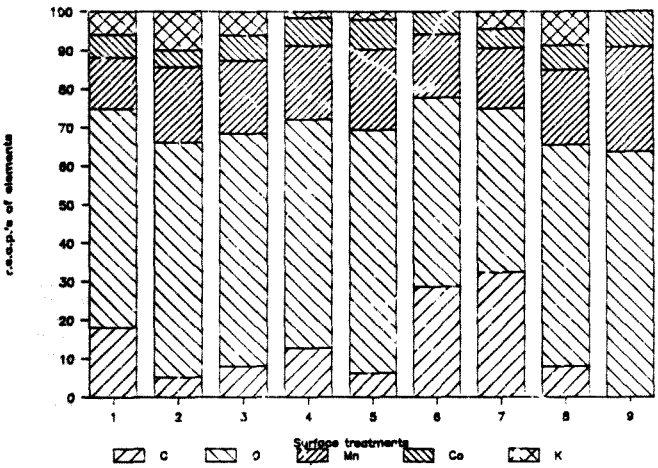

Figure 5.8. Graphic illustration of relative surface atomic percentages of elements between the various treatments, for the CO-hydrogenation study with K-promoted Co/MnO.

	MASS /MASS % HYDROCARBON SELECTIVITY									
TREATMENT	C1	C2=	C2	C3=	C3	C4	C5	C6	MeOH	EtOH
15 min. F-T.	40.5	2.6	6.3	5.5	3.3	10.9	15.3	15.6	TR	TR
1 hour F-T.	34.3	2.33	6.3	7.2	3.6	20.6	8.7	16.9	"	"
3 hours F-T.	64.3	0.5	9.9	0.5	2.2	1.6	0.5	0.4	"	"
6 hours F-T.	40.7	3.8	5.3	7.9	2.6	19.0	8.3	12.5	"	"
12 hours F-T.	62.4	0.7	14.5	2.1	8.1	5.1	3.0	4.1	"	"

Table 5.2. Mass/Mass % of hydrocarbon components detected during various CO-hydrogenation treatments over K-promoted Co/MnO.

Percent potassium promotion		0.25	0.00
Temperature		220°C	220°C
Pressure		500 kPa	500 kPa
GHSV		250 h^{-1}	250 h^{-1}
Percent CO conversion		37.5	37.5
	HYDROCARBON SELECTIVITY (% BY MASS)		
	C1	4.7	8.3
	C2=	2.7	2.3
	C2	0.6	3.5
	C3=	9.9	13.6
	C3	1.8	3.7
	C4	7.9	9.3
	C5+	47.8	38.2
	ALCOHOL SELECTIVITY (% BY MASS)		
	C1	0.3	15.8
	C2	0.8	0.6
	C3	3.6	2.0
	C4	1.3	3.9
	C5	0.4	1.0
	C6	0.6	0.4
	C7	0.9	0.4
	C8	1.7	0.4
	C9	1.1	0.5
	C10+	11.3	8.1
TOTAL % MASS OF ALCOHOLS		20.3	15.8

Table 5.3. Hydrocarbon product distributions obtained from bulk reactor studies during CO-hydrogenation over pure and K-promoted Co/MnO catalysts.

Chapter 6. H_2S poisoning over an industrial iron-based CO-hydrogenation catalyst

6.1. Introduction

It is well known that sulphur compounds rapidly deactivate Fischer-Tropsh catalysts during CO-hydrogenation. Sulphur poisoning of a metal catalyst surface takes place because the adsorption of reactant gases (in this case, H_2 and CO) is prevented, in that the strong metal sulphur bond inhibits co-adsorption of other molecules [98]. Surface poisoning by sulphur is observed at ppb levels and total surface coverages are reached at 250°C to 450°C with P_{H_2S}/P_{H_2} ratios between 10^{-7} and 10^{-10} for cobalt, iron and nickel surfaces [99]. This is explained by the fact that each sulphur atom tends to bond to 3 or 4 metal atoms.

Since electropositive atoms such as the alkali Group I metals are known to promote the activity of metal catalysts, it may be expected that electronegative elements will act as poisons [100]. Sulphur would therefore be expected to lower the catalyst activity by removing electrons [101] whereas K_2O would increase the activity by donating electrons to the metal. This is said to explain why iron-oxide is an inactive F-T synthesis catalyst [5]. The mechanism of sulphur interaction with alkali promoted iron catalysts, is however, poorly understood.

Anderson *et al.* showed that promotion with potassium increased the sulphur resistance of F-T catalysts tenfold [102]. In a review by Maddon and Shaw [103], several patents are mentioned which claim that K_2O promotion is effective for delaying or preventing poisoning by sulphur. Synthesis tests performed by Sasol [5] have however, shown that the amount of CO adsorbed decreases linearly with the amount of H_2S adsorbed. These workers argue that since CO is assumed to selectively chemisorb on the exposed (reduced) iron surface, the above result is said to indicate that H_2S did not combine with surface K_2O in preference to the metallic iron. It should, however, be noted that CO adsorption is strongest at sites promoted by potassium, and a decrease in the number of these sites due to sulphur poisoning could lead to a reduction in the amount of CO adsorbed, thereby masking the "getter" effect of potassium [43].

Re-activation conditions for the catalysts poisoned by sulphur are determined by the metal-sulphur bond characteristics. Re-oxidation has to be carried out at high temperatures, since re-reduction alone leads to a re-distribution of sulphur and no re-activation [104].

6.2. Experimental details

Circular discs of fused magnetite with the following bulk composition (determined by XRF) were used. K_2O (0.58%), CaO (1.13%), MgO (0.74%), Al_2O_3 (1.1%) and SiO_2 (0.74%).

Chapter 2 should be consulted for details of the sample preparation procedures.

The catalyst surface was characterised between various treatments administered in the following sequence:

1. Before treatment
2. Reduction with H_2 (12 hours).
3. 1 hour F-T synthesis. (A)
4. 1 ml H_2S (*ca* room temperature).
5. 1 hour F-T synthesis. (B)
   1 ml H_2S (*ca* 100°C).
6. 1 hour F-T synthesis. (C)
7. 2 ml H_2S (*ca* room temperature).
   1 hour F-T synthesis. (D)
8. Re-reduction with H_2 (12 hours).

Surface characterisation using XPS and AES was carried out before and after treatments (1 to 8, as shown above), which were administered in the high pressure reactor interfaced to the UHV chamber. AES was used to differentiate between iron-rich areas and promoter-rich areas (or inclusions), previously observed on these catalysts [43].

Reduction was performed at 400°C using a pressure of 600 kPa. CO-hydrogenation was performed at 240°C , using a pressure of 600 kPa, up to a total of 4 hours.

1 and 2 ml pulses of 7 ppm H_2S in H_2 were injected into the reactor under 100 kPa pressure without heating the sample. This was achieved using a gas syringe and introducing the gas through a septum fitted to the gas inlet line of the reactor. (See Figure 2.5). H_2S was administered before and after the various stages of F-T synthesis so as to monitor the possible effect of changing the treatment sequence.

GC data were collected at the end of each F-T treatment (A, B, C, and D, as indicated above) so as to ascertain the effect of H_2S on the catalyst hydrocarbon selectivity.

6.3. Results and discussion

The text refers to XPS and AES spectra recorded between the various treatments, as well as tables illustrating the quantified hydrocarbon data, are shown at the end of this chapter.

6.3.1. Reduction and initial CO-hydrogenation

The surface characteristics of these catalysts during reduction and CO-hydrogenation have been extensively studied [43].

Before any treatment was administered to the catalyst, there was a significant amount of carbon present at the surface. The C (1s) signal has a BE of 285.5 eV, and this is assigned to "adventitious" and/or oxygenated hydrocarbon contamination, presumably originating from the cleaning procedure with acetone [43]. The surface concentration of potassium is also high, as witnessed by the large K ($2p_{3/2}$) signal at a BE of 293.6 eV. (This BE can be associated with K^+, since K_2O is added to the catalyst).

Prior to treatments, the iron at the surface is oxidised. This is shown by the broad Fe ($2p_{3/2}$) signal at 711.5 eV and the shape of the O (1s) signal is probably due to the presence of mixed iron oxides.

After 12 hours of reduction with H_2 at 400°C , the surface concentration of all the promoters (except potassium) increases, and this is consistent with previous findings [51]. (See Figures 6.2, 6.4, and 6.5). The iron is almost completely reduced as witnessed by the shift in the Fe ($2p_{3/2}$) peak to a BE of 706.6 eV. This also results in a narrower O (1s) signal, thereby reinforcing the previous assumption regarding the O (1s) signal shape. The reduction treatment lowers the surface concentration of potassium with respect to carbon. Since potassium is known to be mobile over these catalysts, it may be assumed that some of the potassium has migrated into the catalyst bulk. The C (1s) peak shifts to a BE of 284.3 eV, indicating that the surface carbon becomes graphitic. This explains the large amount of carbon present at the surface after reduction, and is consistent with reduction and F-T studies over similar catalysts [43], which show that samples with higher levels of K_2O promotion (0.56%, compared with say, 0.18%) tend to facilitate graphite formation.

After 1 hour of subsequent F-T synthesis, an increase in carbon deposition coupled with a lowering in the K (2p) signal intensity is observed. (See Figure 6.2). The 2:1 doublet of the K (2p) signal is less clear, and the broader K (2p) signal may be ascribed to the formation of potassium hydroxide [41], due to the presence of H_2O formed during the F-T reaction. The initial CO-hydrogenation treatment does not change the appearance of the XPS spectra obtained from the other elements (namely iron, calcium, silicon, aluminium, oxygen and magnesium).

6.3.2. H_2S poisoning during CO-hydrogenation

The carbon deposited at the surface both before and after the administration of H_2S is seen to have a C (1s) BE at 284.2 eV similar to that of graphite. This is consistent with other studies on iron [40] and nickel [94], where potassium was found to accelerate the transition to graphitic carbon.

The K (2p) doublet lineshape is dependent on the order in which the H_2S is introduced over the catalyst. Namely, directly before F-T synthesis over the catalyst, or directly after. When the surface was analysed directly *after* the introduction of H_2S , the K (2p) doublet shape becomes more apparent (see Figure 6.2), and when the surface is analysed directly *after* F-T synthesis, the K (2p) 2:1 doublet shape is not as obvious. (Possible reasons for the behaviour of the potassium are cited below).

The Fe ($2p_{3/2}$) signal at 706.8 eV remains unchanged after H_2S treatments, indicating that no noticeable oxidation of the iron (or iron sulphide formation) takes place under the conditions employed. The XPS signals of the remaining elements do not seem to be affected by the introduction of H_2S . Small amounts of sulphur are detected at a S (2p) BE of $\pm$ 162 eV, indicating that sulphur is indeed present at the surface after the relevant treatments. (See Figure 6.4). The assignment of the S (2p) signals to specific sulphur containing species, is however difficult due to the high sensitivity at which the spectra were recorded and the large amount of resultant noise.

Under the chosen operating conditions, and with the equipment utilised, changes in the catalyst activity could not be determined accurately with GC. The product *selectivity* changes of the catalyst after treatment with H_2S were however, readily observed.

Introduction of H_2S has the effect of modifying the hydrocarbon distribution, in that a general increase in the C_1 and C_2 hydrocarbon production is observed (see Table 6.1). The C_2 and C_3 olefin to paraffin ratios are also lowered (see Table 6.2). These values are seen to fluctuate according to the order in which the H_2S is added (refer to the experimental outline at the beginning of this chapter). The H_2S for treatment 5 was introduced directly after F-T synthesis at 240°C was performed over the catalyst; whilst the H_2S for treatments 4 and 7 were administered directly after surface analysis in the UHV chamber. The result of this is that H_2S for treatment 5 was administered whilst the catalyst was at a higher temperature compared to the other two H_2S treatments. The effect of introducing H_2S at higher temperature is shown in the GC data, where the methane production in the subsequent F-T reaction increases.

From the XPS and GC data, it is clear that when introduced at low levels (and low temperature), the H_2S interacts with potassium (presumably in the form of KOH), and this somehow inhibits, but does not cancel, the role of the potassium promoter. This is shown by the increase in methane production, coupled to decreases in the low molecular weight hydrocarbon olefin/paraffin ratios and lower average hydrocarbon chain-lengths (up to C_6). The fact that this is not a constantly increasing trend, indicates that the catalyst is capable of "recovering" some of it's original selectivity during the F-T reactions. The observation that the catalyst still produces hydrocarbons, even after the final H_2S treatment, coupled to the unchanging Fe ($2p_{3/2}$) signal, is indicative that the

treatment temperatures and sulphur levels are sufficiently low so as to exhibit selective association with potassium centres. Moreover, this assumption is further reinforced by findings that at very low levels of H_2S (13 ppb) in the gas phase, the methanation activity of pure transition metal catalysts decreases by about tenfold, and this is accompanied by an increase in the average hydrocarbon chain-length [99]. This fact is probably not due to electronic interactions, but rather because of geometric blocking of the active sites, and this explaination is in agreement with a recent theoretical study [100].

The changing K (2p) XPS signal, as well as the varying GC data may be correlated with some of the AES data. Previous EDAX (or Energy Dispersive Analysis of X-rays) studies with these catalysts [43], show that the oxide promoters, Al_2O_3, SiO_2, CaO, and K_2O associate to form promoter-rich inclusions over the catalyst, dispersed between iron-rich centres. These promoter-rich inclusions contain potassium silicates.

AES spot analyses performed in this study between the various treatments, show that strong K (LLM) signals originating from a promoter-rich area are associated with lower S (LMM) signals, when compared with iron-rich areas with strong K (LLM) signals. Conversely, iron-rich areas with weak K (LLM) signals (relative to the C (KLL) signal), show very little sulphur deposition. (See Figure 6.7). Since the XPS data shows that sulphur attacks the potassium, the AES data therefore shows that sulphur has a higher affinity towards potassium in the iron-rich areas, compared with the potassium in the promoter-rich areas.

Since it has previously been established that KOH derived from K_2O, is mobile over the entire catalyst surface [105], and that the promoter-rich inclusions contain potassium silicates, the following explanation as to the observed characteristics of the catalyst system between CO-hydrogenation and H_2S treatments is put forward.

It is proposed that sulphur (from the H_2S) interacts with potassium (from KOH) to form a "K_xS_y" alkali-polysulphide complex [106] via an acid-base reaction while the potassium silicate remains intact. This explains the apparent affinity of the sulphur for the potassium associated with iron-rich areas. (As illustrated by the AES data). It is further proposed that water produced by the F-T reactions facilitates leaching of KOH from potassium silicate in the promoter-rich inclusions, thereby countering complete deactivation of the catalyst [107]. (See Figure 6.1). This theory can also be used to

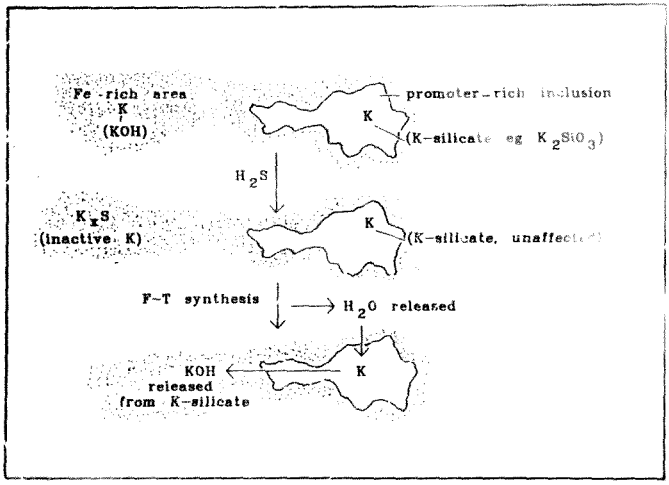

Figure 6.1. Schematic representation of the proposed interaction of H_2S with the industrial iron catalyst.

explain the variable hydrocarbon selectivities observed, in that the role of the potassium is partially restored.

6.3.3. Re-reduction with H_2

Reduction of the treated catalyst has the effect of removing a large portion of the surface carbon. (The C (1s) signal intensity decreases relative to the K (2p) signal). Graphitic carbon with a C (1s) BE of 284.2 eV is left at the surface.

Analysis of the surface after re-reduction (performed at 400 °C) shows that the sulphur is not removed (see Figures 6.4 and 6.7). This is consistent with findings of other workers who claim that a fluidised iron catalyst which has been poisoned by sulphur is not readily reactivated, and that high temperature reduction (up to 450°C) with pure H_2 has no reactivating effect [5].

6.4. Conclusions

When H_2S is introduced over the catalyst under the experimental conditions employed, it selectively attacks potassium centres in KOH, and not the metallic iron centres. This is shown to inhibit the role of the potassium during CO-hydrogenation in that methane selectivity increases, and low molecular weight olefin selectivity declines. The extent of the hydrocarbon selectivity changes are determined by the temperature of the catalyst when the H_2S is injected, in that these changes are more marked when the H_2S is administered at higher temperature.

Based on the XPS, AES and GC results (and incorporating other EDAX findings), a theory on the possible mechanism of H_2 interaction with the catalyst was proposed.

6.5. Data collected for the H_2S poisoning study over an industrial iron catalyst

See following pages.

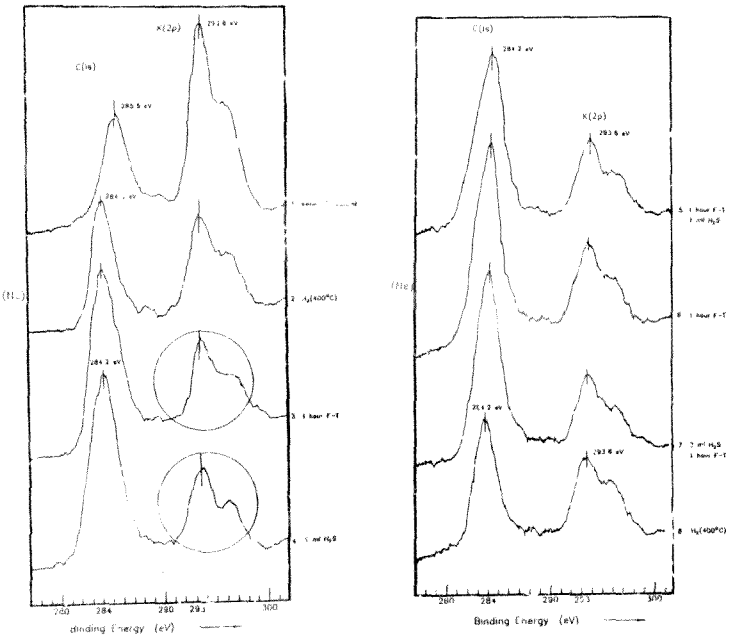

Figure 6.2. XPS spectra recorded in the C (1s) and K (2p) regions between various treatments, for the H_2S poisoning study with an industrial iron catalyst.

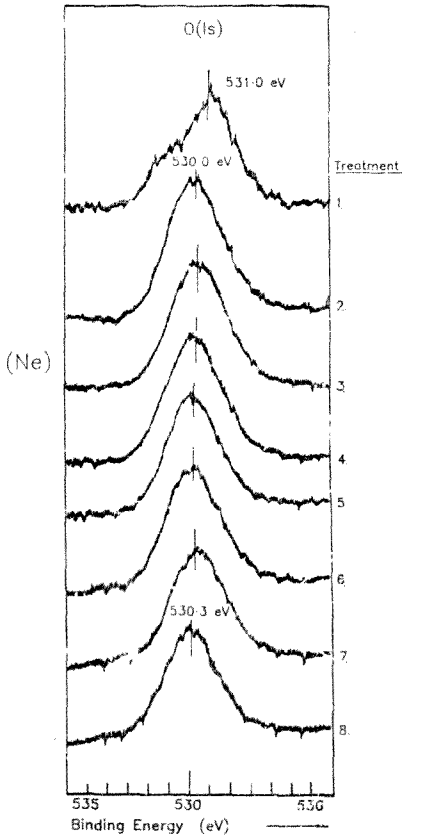

Figure 6.3 XPS spectra recorded in the O (1s) region between various treatments, for the H_2S poisoning study with an industrial iron catalyst.

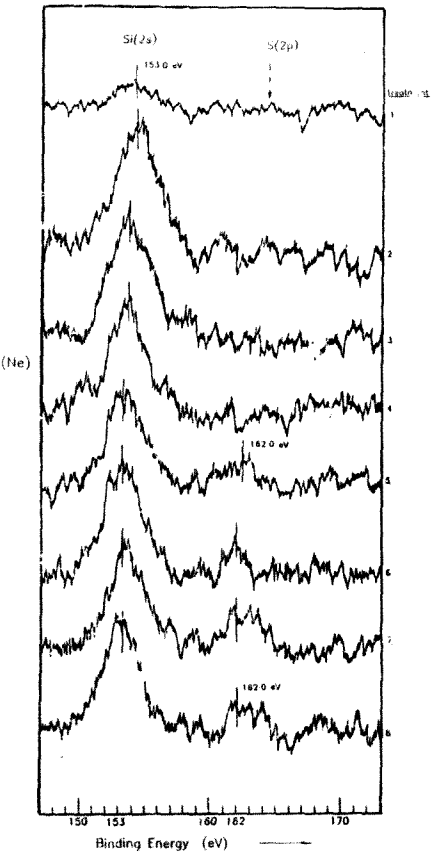

Figure 6.4. XPS spectra recorded in the Si (2s) and S (2p) regions between various treatments, for the H_2S poisoning study with an industrial iron catalyst.

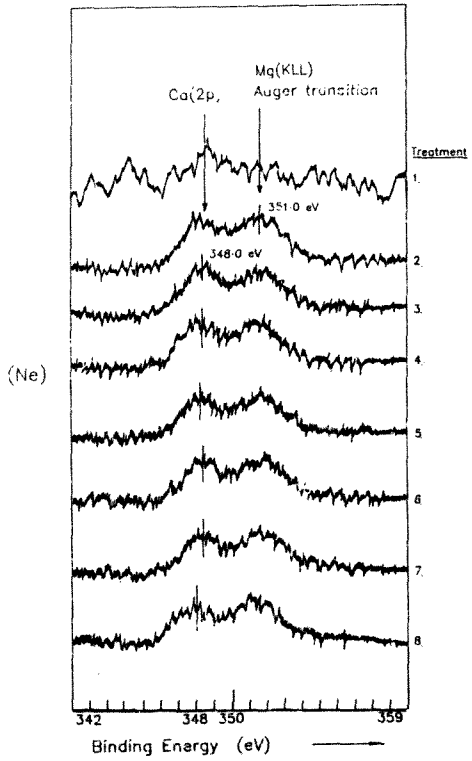

Figure 6.5. XPS spectra recorded in the Ca (2p) region and Mg (KLL) Auger region between various treatments, for the H_2S poisoning study with an industrial iron catalyst.

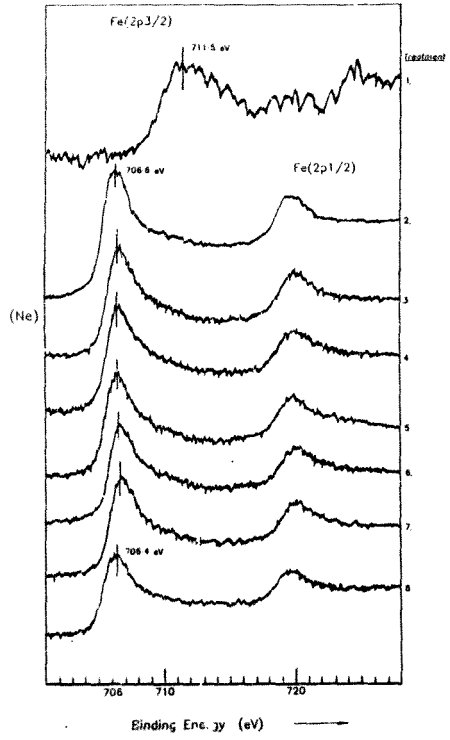

Figure 3.6. XPS spectra recorded in the Fe (2p) region between various treatments, for the H_2S poisoning study with an industrial iron catalyst.

	MASS/MASS % HYDROCARBON SELECTIVITY							
TREATMENT	C1	C2=	C2	C3=	C3	C4	C5	C6
A	37.9	3.3	17.3	6.9	11.1	11.0	6.8	5.7
B	45.7	2.1	20.0	3.9	12.4	8.5	4.4	3.0
C	63.2	3.0	19.5	2.7	6.7	0.3	1.2	3.4
D	51.5	1.9	20.6	2.6	11.5	6.1	3.1	2.7

Table 6.1. Mass/Mass % of hydrocarbon components detected during CO-hydrogenation treatments, for the H_2S poisoning study with an industrial iron catalyst.

	OLEFIN TO PARAFFIN RATIO		
TREATMENT	C2	C3	C4
A	0.20	0.63	0.39
B	0.10	0.32	0.27
C	0.16	0.41	0.39
D	0.10	0.25	0.22

Table 6.2. Olefin to paraffin ratios during CO-hydrogenation treatments, for the H_2S poisoning study with an industrial iron catalyst.

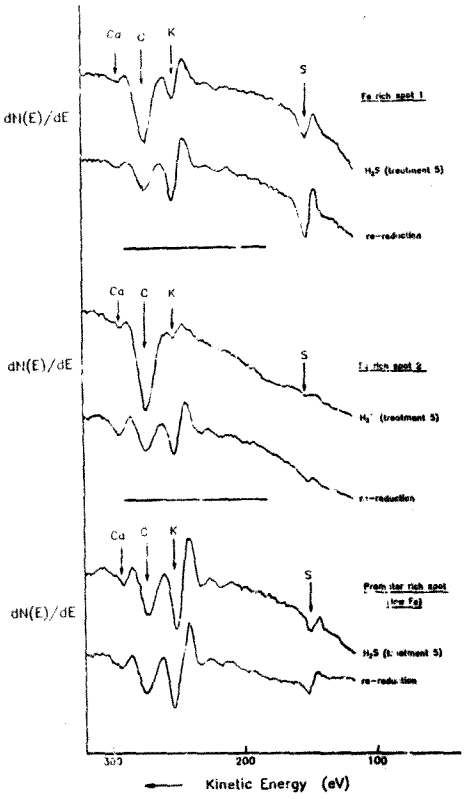

Figure 6.7. AES spectra of Ca (LMM), C (KLL), K (LMM) and S (LMM) transitions from different catalyst regions, for the H_2S poisoning study with an industrial iron catalyst.

Conference proceedings and publications

During the course of this dissertation, some of the work has been presented at symposiums and conferences. Manuscripts for publication are presently being compiled.

Conferences

P.M. Loggenberg, R.G. Copperthwaite, M.J. Betts and J.P.F. Sellschop, "A Surface Study of the CO-hydrogenation Reaction", Inorganic '88 Conference, Gordons Bay (RSA), April 1988.

M.J. Betts and R.G. Copperthwaite, "Surface Studies of Co/MnO Catalysts", National Physical Chemistry Symposium of the South African Chemical Institute, Dikhololo Bushveld Villas (RSA), July 1988.

M.J. Betts and R.G. Copperthwaite, "Surface Studies on Co/Mn Fischer-Tropsch Catalysts", Annual Meeting: Catalysis and Catalytic Reactor Technology in the RSA, Vereeniging (RSA), August 1988.

M.J. Betts, R.G. Copperthwaite and P.M. Loggenberg, "Sulphur Poisoning Experiments on Fischer-Tropsch Catalysts", 30th Convention of the South African Chemical Institute, Johannesburg, January 1989.

Publications

References

[1] P.Sabatier and J.B. Senderens, Hebd. Seances Acad. Sci., **134**, (1902), 514.

[2] BASF: German Pat. 293, (1913), 787.

[3] F. Fischer and H. Tropsch, Brenst. Chem. **4**, (1923), 276

[4] F. Fischer and H. Tropsch, Brenst. Chem. **7**, (1926), 97.

[5] M.E. Dry, in "Catalysis, Science and Technology Vol. 1", (Eds. J.R. Anderson and M. Boudart, Springer, Berlin, 1981).

[6] H. Pichler, "Advan. Catal. Vol. 4", (Eds. Frankenburg, Komarewsky and Rideal, Academic Press Inc., New York, 1952).

[7] H.H. Storch, N. Golumbic and R.B. Anderson, in "The Fischer-Tropsch and Related Synthesis.", (John Wiley, New York, 1951).

[8] R.B. Anderson, in "Catalysis, Vol. IV", (Ed. P.H. Emmett, Reinhold, New York, 1986).

[9] R.B. Anderson, "Advan. Catal. Vol. 5", (Eds. Frankenburg, Komarewsky and Rideal, Academic Press Inc. New York, 1953).

[10] G.V. Schulz, Z. Phys. Chem. Abt. B. **30**, (1935), 379.

[11] P.J. Flory, J. Amer. Chem. Soc., **58**, (1936), 1877.

[12] E.L. Muetterties and J. Stein, Chem. Rev., **79 (6)**, (1979), 479.

[13] R.C. Brady and R. Petit, J. Amer. Chem. Soc. **102**, (1980), 6182.

[14] R.C. Brady and R. Petit, J. Amer. Chem. Soc. **103 (5)** , (1981), 1289.

[15] W.A. Herrmann, Angew. Chem. Int. Ed. Engl., **21**, (1982), 117.

[16] G. Henrici-Olivé and S. Olivé, in "The chemistry of the hydrogenation of carbon monoxide", (Springer, New York, 1984).

[17] K. Roder and H. Werner, Angew. Chem. Int. Ed. Engl., **26 (7)** 686.

[18] J.T. Kummer and P.H. Emmet, J. Amer. Chem. Soc., **75**, (1953), 5177.

[19] V.V. Voevodski, F.F. Volkenshtein and N.N. Semenov, Proc. All Union Conf.-Probl. Chem. Kin. Catal. and Reactiv., Izd. Akad. Nauk. SSR, Moscow, (1955), 423.

[20] S. Hamai, J. Chem. Soc. Jpn., **62**, (1941), 516.

[21] A. Ekstroom and J.A. Lapszewicz, J. Phys. Chem., **91**,(1987), 4514.

[22] H. Pichler and H. Schulz, Chem. Ing. Tech., **42**, (1970), 1162.

[23] C.K. Rofer-De Poorter, Chem. Rev., **81**, (1981), 447.

[24] G. Henrici-Olivé and S. Olivé, in "The Chemistry of the Metal-Carbon Bond, Vol. 3" (Eds. Hartley and Patai, J. Wiley and sons, New York 1985), 391.

[25] R.W.G. Wykoff and E.D. Crittenden, J. Amer. Chem. Soc., **47**, (1925), 2866.

[26] A. Ozaki and K. Aika, in "Catalysis, Science and Technology, Vol. 1", (Eds. J.R. Anderson and M. Boudart, Springer, Berlin, 1981).

[27] M.E. Dry, J.A.K. du Plessis and G.M. Leuteritz, J. Catal., **6**, (1966), 194.

[28] R.G. Copperthwaite, (University of the Witwatersrand), personal communication, October 1988.

[29] G. Ertl and J. Küppers, in Low Energy Electrons and Surface Chemistry, 2nd Ed., (VCH Verlagsgesellschaft, Weinheim, Fed. Rep. Ger., 1985).

[30] T.A. Carlson, in "Photoelectron and Auger Spectroscopy, 2nd. Ed.", (Plenum Press, New York, 1978).

[31] D. Briggs and M.P. Seah, in "Practical Surface Analysis by Auger and X-ray Photoelectron Spectroscopy", (John Wiley and Sons, New York, 1983).

[32] K. Siegbahn *et al.*, "ESCA-Atomic, Molecular and Solid State Structure Studied by Means of Electron Spectroscopy", (Almquist and Wicksell, Uppsala, 1967).

[33] M.W. Roberts, Sci. Prog., Oxf., 65, (1982), 67.

[34] M.P. Seah and W.A. Dench, NPL Report Chem., (1978), 82.

[35] P. Auger, J. Phys. Radium, **6**, (1925), 205.

[36] M. van der Riet, Ph.D. Thesis, University of the Witwatersrand, Johannesburg, RSA, (1988).

[37] J. Barrault, in "Metal Support and Metal Additive Effects in Catalysis", (Ed. B. Imelik, Elsevier, Amsterdam, 1982), 225.

[38] M. Muhler, R. Schlögl, S.Erder and G. Ertl, Surf. Sci., **189/190**, (1987), 69.

[39] D.W. Blakely, E. Kozak, B.A. Sexton and G.A. Somorjai, J. Vac. Sci. Technol., **13**, (1976), 1901.

[40] D.A. Wesner, F.P Coenen, and H.P. Bonzel, Langmuir, **1**, (1985), 487.

[41] D.J. Dwyer and J.H. Hardenbergh, J. Cat., **87**, (1984), 66.

[42] R.G. Copperthwaite, P.M. Loggenberg, T.E. Derry and J.F.P. Sellschop , Vacuum, **38**, (1988), 413.

[43] P.M. Loggenberg, Ph.D. Thesis, University of the Witwatersrand, Johannesburg, RSA, (1989).

[44] De Beers, S.A. patent, provisional patent 88-2028

[45] P.M. Loggenberg (University of the Witwatersrand), personal communication, May (1988).

[46] M. van der Riet, G.J. Hutchings and R.G. Copperthwaite, J. Chem. Soc., Chem. Commun., (1986), 798.

[47] R.G. Copperthwaite, G.J. Hutchings and M. van der Riet, S.A. Journal of Sci., **82**(1986), 596.

[48] G.C. Maiti, R. Malessa and M. Baerns, Appl. Catal., **5**, (1981) , 151.

[49] S.E. Colley, (University of the Witwatersrand), personal communication, June 1988.

[50] S.E. Colley, R.G. Copperthwaite, G.J. Hutchings and M. van der Riet, Ind. Eng. Chem. Res., **27**, (1987), 1339.

[51] P.M. Lorgenberg, R.G. Copperthwaite, R.C. Everson and J.P.F. Sellschop, Appl. Surf. Sci., **31**, (1988), 377.

[52] D. Vermaire (Sastech), personal communication, October 1988.

[53] W.A. Dietz, J. of Gas Chromatogr., (1967), 68.

[54] R.G. Copperthwaite, H. Hack, G.J. Hutchings and J.P.F. Sellschop, Surf. Sci. Letters, **164**, (1985), 827.

[55] M.W. Roberts and R.St.C. Smart, Chem. Phys. Letters, **69**, (1980), 234.

[56] S.R. Keleman, A. Kaldor and D.J. Dwyer, Surf. Sci., **121**, (1982), 45.

[57] T.E. Madey, J.T. Yates Jr. and N.E. Erickson, Chem. Phys. Lett., **19**, (1973), 487.

[58] A.F. Carley and M.W. Roberts, Proc. R. Soc. Lond. A. **363**, (1978), 403.

[59] M.P. Seah and W. Dench, Surf. Interface Anal., **1**, (1979), 2.

[60] D.R. Penn, J. of Elec. Spectrosc. and Rel. Phenom., **8**, (1976), 29.

[61] J.H. Schofield, J. of Elec. Spectrosc. and Rel. Phenom., **9**, (1976), 129.

[62] T. Grzybek, H. Papp and M. Baerns, Appl. Catal., **29**, (1987), 335.

[63] G.C. Allen, S.J. Harris, J.A. Jutson and J.M. Dyke, Appl. Surf. Sci., **37** (1), (1989), 111 .

[64] S.J. Cochran and F.P. Larkins, J. Chem. Soc., Faraday Trans. 1, **85**, (1985), 2179.

[65] D.J. Dwyer and J.H. Hardenberg, Appl. Surf. Sci., **19**, (1984), 1466.

[66] N.S. McIntyre and M.G. Cook, Anal. Chem., **47**, (1975), 2208.

[67] C.R. Brundle, T.J. Chuang and D.W. Rice, Surf. Sci., **60**, (1976), 286.

[68] J.C. Fuggle, J. Elec. Spectrosc. Rel. Phenom., **21**, (1980), 275.

[69] G.C. Maiti, R. Malessa and M. Baerns, Appl. Catal., **5**, (1983), 151.

[70] G.C. Maiti, R. Malessa, U. Löchner, H. Papp and M. Baerns, Appl. Catal., **16**, (1985), 215.

[71] N.K. Jaggi, L.H. Schwartz, J.B. Butt, H. Papp and M. Baerns, Appl. Catal., **13**, (1985), 347.

[72] U. Löchner, H. Papp and M. Baerns, Appl. Catal., **23**, (1986), 339.

[73] H.-J. Engell, K. Bohnenkamp, M.K. Kohl, E. Riecke and K.-H. Ulrich, in "Über die Reduktion von Wüstit, Magnetit und Eisen-Mangan Mischoxyden", Forschungsberichte des Landes Nordrhein-Westfalen, Nr. 1909, (Westdeutscher Verlag, Köln und Opladen, 1968).

[74] H.-J. Engell and K.H. Kohl, Z. for Elektroch., **66**, (1962), 684.

[75] H. Schmalzried, Ber. Bunsenges. Phys. Chem., **88**, (1984), 1186.

[76] D.A. Wesner, G. Linden and H.P. Bonzel, Appl. Surf. Sci., **26**, (1986), 335.

[77] L. Gonzalez, R. Miranda and S. Ferer, Surf. Sci., **119**, (1982), 61.

[78] W.L. van Dijk, J.W. Niemansverdriet, A.M. van der Kraan and H.S. van der Baan, Appl. Catal., **2**, (1982), 273.

[79] F. Steinbach, J. Kiss and R. Krall, Surf. Sci., **157**, (1985), 401.

[80] T. Grzybek, H. Papp and M. Baerns, Appl. Catal., **29**, (1987), 351.

[81] C. A. Mims, Catal. Lett., **1**, (1988), 293.

[82] R.G. Copperthwaite, G.J. Hutchings and M. van der Riet, Roy. Soc. Chem., Faraday Discussion Meeting, Bath (UK), September 1986.

[83] H.P. Bonzel and H.J. Krebs, Surf. Sci., **91**, (1980), 499.

[84] H.J. Krebs and H.P. Bonzel, Surf. Sci., **99**, (1980), 570.

[85] S.E. Colley, R.G. Copperthwaite, G.J. Hutchings, S.P. Terblanche and M.M. Thackeray, Nature, **339** (6220) , (1989), 129.

[86] H. Matsumoto and C.O. Bennet, J. Catal., **53**, (1978), 331.

[87] S.E. Colley, personal communication, 1989.

[88] T. Themistocleous (University of the Witwatersrand), personal communication, 1989.

[89] S.R. Keleman, A. Kaldor and D.J. Dwyer, Surf. Sci., **121**, (1982), 45.

[90] M. Muhler, R.Schlögl, S. Eder and G. Ertl., Surf. Sci., **189/190**, (1987), 69.

[91] H.P. Bonzel, G. Broden and H.J. Krebs, Appl. Surf. Sci., **16**, (19 373.

[92] J.E. Crowell, E.L. Garfunkel and G.A. Somorjai, Surf. Sci., **121**, (1982), 303

[93] M.P. Kiskonova, Surf. Sci., 111, (1981), 584.

[94] C.T. Campbell and D.W. Goodman, Surf. Sci., **123**, (1982), 413.

[95] A. Ozaki and K. Aika, in "Catalysis, Science and Technology, Vol. 1.", (Eds. J.R. Anderson and M. Boudart, Springer, Berlin, 1981), 87.

[96] G.A. Somorjai, Surf. Sci., **89**, (1979), 496.

[97] G.A. Somorjai, Catalysis Rev.-Sci. Eng., **23**, (1981), 189.

[98] C.H. Bartholemew, P.K. Agrawal and J.R. Katzer, Adv. Catal., **32**, (1982), 136

[99] P.K. Agrawal, W.D. Fitzharris and J.R. Katzer, in "Catalyst Deactivation", (Eds. B. Delmon and G.F. Fromet, Elsevier, Amsterdam, 1980), 179.

[100] N.D. Lang, S. Holloway and J.K. Nørskov, Surf. Sci., **150**, (1985), 24.

[101] E. Einkeev, A.V. Krylova, Kinet. Katal., **3**, (1962), 116.

[102] R.B. Anderson, F.S. Karn and J.F. Schultz, J. Catal., **4**, (1965), 56.

[103] R.J. Madon and H. Shaw, Catal. Rev., **15 (1)**, (1977), 69.

[104] R.B. Anderson, in "Catalysis Vol. IV", (Ed. P.H. Emmett, New York, Reinhold, 1956).

[105] T. Grzybek, H. Papp and M. Baerns, Appl. Catal., **29**, (1987), 335.

[106] F.A. Cotton and G. Wilkinson, in "Advanced Inorganic Chemistry, 3rd. Ed.", (Interscience, New York, 1972), 431.

[107] P.M. Loggenberg (Sastech), personal communication, 1989.